

Structure-Preserving High-Order Methods for the Compressible Euler Equations in Potential Temperature Formulation for Atmospheric Flows

Marco Artiano^{*1}, Oswald Knoth², Peter Spichtinger^{†3}, and Hendrik Ranocha^{‡1}

¹Institute of Mathematics, Johannes Gutenberg University Mainz, Germany

²Leibniz Institute for Tropospheric Research (TROPOS), Leipzig, Germany

³Institute for Atmospheric Physics, Johannes Gutenberg University Mainz, Germany

September 23, 2025

Abstract

We develop structure-preserving numerical methods for the compressible Euler equations, employing potential temperature as a prognostic variable. We construct three numerical fluxes designed to ensure the conservation of entropy and total energy within the discontinuous Galerkin framework on general curvilinear meshes. Furthermore, we introduce a generalization for the kinetic energy preservation property and total energy conservation in the presence of a gravitational potential term. To this end, we adopt a flux-differencing approach for the discretization of the source term, treated as non-conservative product. We present well-balanced schemes for different constant background states for both formulations (total energy and potential temperature) on curvilinear meshes. Finally, we validate the methods by comparing the potential temperature formulation with the traditional Euler equations formulation across a range of classical atmospheric scenarios.

Key words. structure-preserving methods, discontinuous Galerkin methods, flux differencing, well-balanced schemes, entropy conservation, entropy-stable methods, kinetic energy preservation, pressure equilibrium preservation

AMS subject classification. 65M12, 65M20, 65M70, 65M60, 65M06

1 Introduction

Discontinuous Galerkin (DG) methods have gained significant attention for hyperbolic equations due to their ability to accurately capture complex fluid and wave phenomena in applications such as atmospheric physics. Their compact formulation enables excellent parallel scalability, making them suitable for high-resolution simulations [39]. However, DG methods often require additional stabilization when handling discontinuities or under-resolved features. Especially in atmospheric simulations, to keep stability for long-time simulations, filters are applied [24], as well as other classical techniques such as over-integration (dealiasing) [38] and artificial viscosity [62, 68]. While effective, these approaches can reduce accuracy and require parameter tuning. To address these issues, entropy-stable (ES) DG schemes have been developed, offering high-order accuracy with guaranteed nonlinear stability without requiring additional parameters [37, 57, 63, 67]. An essential ingredient of these high-order DG schemes is the implementation of carefully constructed two-point fluxes for the volume terms, an approach pioneered in the context of DG methods by Carpenter et al. [8, 9], Fisher et al. [19], and Gassner et al. [21].

The compressible Euler equations admit several formulations, and it is not entirely clear whether one formulation offers significant advantages over the others. In the computational fluid dynamics (CFD) community, considerable effort has been devoted to the development of structure-preserving schemes using the total energy as state variable [10, 29, 30, 37, 43, 45, 55, 57, 63]. In contrast, the use of potential temperature is especially popular in atmospheric models, where it also plays an important theoretical role in meteorology. Giraldo et al. [24] and more recently Girfoglio et al. [25] have analyzed different formulations for DG and spectral element methods

^{*}ORCID: 0009-0009-5872-702X

[†]ORCID: 0000-0003-4008-4977

[‡]ORCID: 0000-0002-3456-2277

(SEMs) and different pressure-based solvers for the finite volume framework, respectively. In atmospheric applications, the presence of the gravitational potential is crucial for designing well-balanced schemes that preserve the hydrostatic equilibrium [11, 37, 63]. Additional desirable properties in the flux-differencing framework include the preservation of kinetic and potential energy (KPEP), as introduced by Souza et al. [57].

In this work, we focus on the potential temperature formulation to investigate structure-preserving properties, in particular pressure equilibrium preserving (PEP). We design new two-point fluxes that guarantee conservation of either total energy (TEC) or thermodynamic entropy (EC). Building on the ideas in [57, 63], we generalize KPEP, introduce the condition for total energy conservation in presence of a geopotential, and propose a new well-balanced scheme by discretizing the source term as non-conservative product; all these properties are established for both the potential temperature and the total energy formulations. Furthermore, we extend them to the DGSEM [34] using arbitrary curvilinear coordinates.

The paper is organized as follows. We introduce the Euler equations in the potential temperature formulation in Section 2 and derive novel EC and TEC two-point fluxes. Section 3 analyzes their structure-preserving properties, and discusses positivity of pressure and density. Section 4 presents the generalization of KPEP and TEC for flux differencing, and the new well-balanced scheme. Section 5 considers the DGSEM in one dimension on Cartesian grids, while Section 6 generalizes these flux differencing properties to three-dimensional DGSEM on curvilinear meshes. Finally, in Section 7 we report the numerical results comparing different formulations and two-point fluxes. We summarize our results in Section 8.

2 Total energy and entropy-conservative fluxes

The compressible Euler equations with the total energy as conservative variable read

$$\begin{aligned}\partial_t \varrho + \nabla \cdot (\varrho \mathbf{V}) &= 0, \\ \partial_t (\varrho \mathbf{V}) + \nabla \cdot (\varrho \mathbf{V} \otimes \mathbf{V}) + \nabla p &= -\varrho \nabla \phi, \\ \partial_t (\varrho E) + \nabla \cdot ((\varrho E + p) \mathbf{V}) &= -\varrho \mathbf{V} \cdot \nabla \phi,\end{aligned}\tag{1}$$

where ϱ is the density, \mathbf{V} the velocity, ϱE is the sum of kinetic and internal energy, p the pressure, and $\phi = \phi(x, y, z)$ is the gravitational potential. We use an ideal gas equation of state, i.e., $\varrho E = \frac{p}{\gamma-1} + \frac{1}{2} \varrho \|\mathbf{V}\|^2$, where γ is the ratio of specific heats. In the context of local weather prediction and numerical methods for atmospheric applications, the evolution of ϱE is often substituted with the evolution of the potential temperature θ , i.e.,

$$\begin{aligned}\partial_t \varrho + \nabla \cdot (\varrho \mathbf{V}) &= 0, \\ \partial_t (\varrho \mathbf{V}) + \nabla \cdot (\varrho \mathbf{V} \otimes \mathbf{V}) + \nabla p &= -\varrho \nabla \phi, \\ \partial_t (\varrho \theta) + \nabla \cdot (\varrho \theta \mathbf{V}) &= 0,\end{aligned}\tag{2}$$

where $p = p_0 (R\varrho\theta/p_0)^\gamma$, R is the ideal gas law constant, and p_0 is the atmospheric pressure, which we assume to be 100 000 Pa throughout this study. For smooth solutions, the conservative parts of the systems of equations (1) and (2) induce additional scalar conservation laws, which are of the form

$$\partial_t U + \nabla \cdot F(U) = 0,\tag{3}$$

where U is a mathematical entropy functional and F the corresponding flux. For the total energy formulation (1), we use the thermodynamic entropy

$$U_{\varrho s} = \varrho s = \varrho \log \left(\frac{p}{\varrho^\gamma} \right).\tag{4}$$

Usually, this quantity is set as an entropy functional for the derivation of entropy-conservative (EC) or entropy-stable (ES) two-point fluxes. However, considering the conservative part of the system of our interest (2), ϱE (which coincides with the total energy in the absence of the geopotential term) is not a linear invariant. Therefore, we are interested in the construction of two-point numerical fluxes when either the thermodynamic entropy or the total energy are treated as entropy functional, i.e., we consider the mathematical entropies

$$U_{\varrho s} = \varrho s \quad \text{or} \quad U_{\varrho E} = \varrho E.\tag{5}$$

2.1 Entropy analysis

We consider the systems in 1D without gravity (the generalization to multiple dimensions is straightforward), i.e., hyperbolic conservation laws of the form

$$\partial_t \mathbf{u} + \partial_x \mathbf{f}(\mathbf{u}) = 0.\tag{6}$$

A semi-discrete finite volume (FV) method for (6) reads

$$\partial_t \mathbf{u}_i + \frac{1}{\Delta x} (\mathbf{f}^{\text{num}}(\mathbf{u}_i, \mathbf{u}_{i+1}) - \mathbf{f}^{\text{num}}(\mathbf{u}_{i-1}, \mathbf{u}_i)) = 0. \quad (7)$$

From hereinafter, if not stated otherwise, we always consider the right interface at the i -th cell, i.e., $\mathbf{f}^{\text{num}} := \mathbf{f}^{\text{num}}(\mathbf{u}_i, \mathbf{u}_{i+1})$. Moreover, we use the classical operators

$$\begin{aligned} \llbracket a \rrbracket &= a_{i+1} - a_i, & (\text{jump}) \\ \{\{a\}\} &= \frac{a_{i+1} + a_i}{2}, & (\text{arithmetic mean}) \\ \{\{a\}\}_{\log} &= \frac{\llbracket a \rrbracket}{\llbracket \log a \rrbracket}, & (\text{logarithmic mean, cf. [29]}) \\ \{\{a\}\}_{\text{geo}} &= \sqrt{a_{i+1} a_i}, & (\text{geometric mean}) \\ \{\{a\}\}_{\gamma} &= \frac{\gamma - 1}{\gamma} \frac{\llbracket a^\gamma \rrbracket}{\llbracket a^{\gamma-1} \rrbracket}, & (\text{Stolarsky mean, cf. [64]}) \end{aligned} \quad (8)$$

with the well-known properties

$$\llbracket ab \rrbracket = \{\{a\}\} \llbracket b \rrbracket + \{\{b\}\} \llbracket a \rrbracket, \quad \llbracket a^2 \rrbracket = 2 \llbracket a \rrbracket \{\{a\}\}, \quad \llbracket 1/a \rrbracket = -\frac{\llbracket a \rrbracket}{\{\{a\}\}_{\text{geo}}^2}. \quad (9)$$

Let (U, F) denote a mathematical entropy-entropy flux pair for (6).

Definition 2.1 (Tadmor [58, 59]). A two-point numerical flux \mathbf{f}^{num} is EC for a given entropy U if

$$\llbracket \boldsymbol{\omega}^T \rrbracket \mathbf{f}^{\text{num}} - \llbracket \psi \rrbracket = 0, \quad (10)$$

where $\boldsymbol{\omega} = U'$ are the entropy variables and $\psi = \boldsymbol{\omega}^T \mathbf{f} - F$ is the flux potential.

It is of particular interest that the Hessian of the total energy and of the thermodynamic entropy, when expressed with respect to $\mathbf{u} = (\varrho, \varrho v, \varrho \theta)$, are given by

$$U''_{\varrho E}(\mathbf{u}) = \begin{bmatrix} m^2/\varrho^3 & -m/\varrho^2 & 0 \\ -m/\varrho^2 & 1/\varrho & 0 \\ 0 & 0 & K\gamma(\varrho\theta)^{\gamma-2} \end{bmatrix}, \quad U''_{\varrho s}(\mathbf{u}) = \begin{bmatrix} \frac{\gamma}{\varrho} & 0 & -\frac{\gamma}{\varrho\theta} \\ 0 & 0 & 0 \\ -\frac{\gamma}{\varrho\theta} & 0 & \frac{\gamma\varrho}{(\varrho\theta)^2} \end{bmatrix}, \quad (11)$$

with eigenvalues

$$\lambda_{\varrho E,1} = 0, \quad \lambda_{\varrho E,2} = \frac{m^2 + \varrho^2}{\varrho^3}, \quad \lambda_{\varrho E,3} = K\gamma(\varrho\theta)^{\gamma-2}, \quad (12)$$

$$\lambda_{\varrho s,1} = \lambda_{\varrho s,2} = 0, \quad \lambda_{\varrho s,3} = \frac{\gamma}{\varrho} + \gamma \frac{\varrho}{\varrho\theta}. \quad (13)$$

Both Hessians are positive semidefinite, which implies that the entropy functionals are merely convex. As a consequence, the mapping between the conserved and the entropy variables is no longer one-to-one [26], in both cases. Nonetheless, strict convexity is not required for Tadmor's analysis to hold, as the conditions stated in Definition 2.1 are still valid. Therefore, this does not preclude the development of total energy-conservative (TEC) and thermodynamic entropy-conservative (EC) numerical fluxes, presented in the next sections. On the other hand, the conditions of Barth's Theorem [4] cannot be directly applied to uniquely determine a dissipation operator [65]; as a result the construction of such operators is not straightforward.

2.2 Derivation of a TEC flux

Next we use the total energy $U_{\varrho E} = \varrho E$ as mathematical entropy for the system (2) without gravity. Thus, given the set of conservative variables $\mathbf{u} = (\varrho, \varrho v, \varrho \theta)$, we look for a numerical flux mimicking at the discrete level the conservation of the total energy, given in (1). By introducing the conserved variables

$$\mathbf{u} = (\varrho, \varrho v, \varrho \theta) = (\varrho, m, \varrho \theta), \quad (14)$$

we can rewrite the mathematical entropy (total energy) and the corresponding flux as

$$U_{\varrho E} = \varrho E = K \frac{(\varrho\theta)^\gamma}{\gamma - 1} + \frac{1}{2} \frac{m^2}{\varrho}, \quad F_{\varrho E} = (U_{\varrho E} + K(\varrho\theta)^\gamma) \frac{m}{\varrho}, \quad (15)$$

where $K = p_0(R/p_0)^\gamma$. Thus, the mathematical entropy variables and the associated flux potential are

$$\omega^T = \left(-\frac{1}{2} \frac{m^2}{\varrho^2}, \frac{m}{\varrho}, \frac{\gamma}{\gamma-1} K(\varrho\theta)^{\gamma-1} \right), \quad \psi = K(\varrho\theta)^\gamma \frac{m}{\varrho}. \quad (16)$$

Applying the general Tadmor EC condition (10) to $U_{\varrho E} = \varrho E$, we obtain

$$-\frac{1}{2} \left[\frac{m^2}{\varrho^2} \right] f_\varrho^{\text{num}} + \left[\frac{m}{\varrho} \right] f_{\varrho v}^{\text{num}} + \frac{\gamma}{\gamma-1} K \left[(\varrho\theta)^{\gamma-1} \right] f_{\varrho\theta}^{\text{num}} - K \left[(\varrho\theta)^\gamma \frac{m}{\varrho} \right] = 0, \quad (17)$$

and we refer to (17) as the total energy-conservative (TEC) condition. To derive a TEC flux, we compute the jumps of the entropy variables in (17) by recursively applying the discrete operators (8) and (9) as follows:

$$\begin{aligned} \llbracket \psi \rrbracket &= \left[K(\varrho\theta)^\gamma \frac{m}{\varrho} \right] = \llbracket K(\varrho\theta)^\gamma \rrbracket \left\{ \left\{ \frac{m}{\varrho} \right\} \right\} + \{ \{ K(\varrho\theta)^\gamma \} \} \left[\frac{m}{\varrho} \right] \\ &= K \llbracket (\varrho\theta)^\gamma \rrbracket \left\{ \left\{ \frac{m}{\varrho} \right\} \right\} + K \{ \{ (\varrho\theta)^\gamma \} \} \left(\llbracket m \rrbracket \left\{ \left\{ \frac{1}{\varrho} \right\} \right\} - \frac{\{ \{ m \} \} \llbracket \varrho \rrbracket}{\{ \{ \varrho \} \}_{\text{geo}}^2} \right), \end{aligned} \quad (18)$$

$$\llbracket \omega_1 \rrbracket = - \left\{ \left\{ \frac{m}{\varrho} \right\} \right\} \left(\llbracket m \rrbracket \left\{ \left\{ \frac{1}{\varrho} \right\} \right\} - \frac{\{ \{ m \} \} \llbracket \varrho \rrbracket}{\{ \{ \varrho \} \}_{\text{geo}}^2} \right), \quad (19)$$

$$\llbracket \omega_2 \rrbracket = \llbracket m \rrbracket \left\{ \left\{ \frac{1}{\varrho} \right\} \right\} - \frac{\{ \{ m \} \} \llbracket \varrho \rrbracket}{\{ \{ \varrho \} \}_{\text{geo}}^2}, \quad (20)$$

$$\llbracket \omega_3 \rrbracket = \frac{\gamma}{\gamma-1} K \llbracket (\varrho\theta)^{\gamma-1} \rrbracket. \quad (21)$$

By substituting all terms into the entropy conservation condition and requiring that each coefficient of the jumps vanishes, we obtain

$$\begin{aligned} \left\{ \left\{ \frac{m}{\varrho} \right\} \right\} \{ \{ m \} \} f_\varrho^{\text{num}} - \{ \{ m \} \} f_{\varrho v}^{\text{num}} + K \{ \{ (\varrho\theta)^\gamma \} \} \{ \{ m \} \} &= 0, \\ f_{\varrho v}^{\text{num}} &= \left\{ \left\{ \frac{m}{\varrho} \right\} \right\} f_\varrho^{\text{num}} + K \{ \{ (\varrho\theta)^\gamma \} \}, \\ \left(\frac{\gamma}{\gamma-1} \llbracket (\varrho\theta)^{\gamma-1} \rrbracket \right) f_{\varrho\theta}^{\text{num}} &= \llbracket (\varrho\theta)^\gamma \rrbracket \left\{ \left\{ \frac{m}{\varrho} \right\} \right\}. \end{aligned} \quad (22)$$

By substituting the second into the first equation, one can verify that it is always satisfied, leading to a degree of freedom in the density flux. Hence, we can state the following result:

Theorem 2.2. *A numerical flux for the compressible Euler equations in potential temperature formulation satisfying*

$$f_{\varrho v}^{\text{num}} = \left\{ \left\{ \frac{m}{\varrho} \right\} \right\} f_\varrho^{\text{num}} + \{ \{ p \} \}, \quad f_{\varrho\theta}^{\text{num}} = \{ \{ \varrho\theta \} \}_\gamma \left\{ \left\{ \frac{m}{\varrho} \right\} \right\}, \quad (23)$$

where f_ϱ^{num} is any consistent and symmetric discretization of $m = \varrho v$, is TEC.

We now turn our attention to the derivation of thermodynamic entropy-conservative numerical fluxes and, in particular, how to choose the degree of freedom given by the density flux.

2.3 Conservation of the thermodynamic entropy

In the development of EC fluxes for compressible Euler equations, a common approach involves deriving these fluxes so that ϱs is conserved at a semi-discrete level [10, 29, 43]. This is the first step towards the development of ES fluxes [63, 65].

In contrast to the previous section, where the total energy has been treated as a mathematical entropy, we focus on the thermodynamic entropy and derive numerical fluxes that conserve it at the semi-discrete level. Since the procedure is analogous to the previous section, we highlight only the main steps in the derivation. We start considering the set of variables $\mathbf{u} = (\varrho, \varrho v, \varrho\theta)$ and the entropy functional $U_{\varrho s}$. The associated entropy variables are

$$\omega_{\varrho s}^T = \left(\log\left(\frac{K(\varrho\theta)^\gamma}{\varrho^\gamma}\right) - \gamma, 0, \gamma \frac{\varrho}{\varrho\theta} \right). \quad (24)$$

Following the same steps for the TEC flux, the potential flux for this case reduces to $\psi = 0$. Consequently, we have that a numerical flux $f^{\text{num}} = (f_\rho^{\text{num}}, f_{\rho v}^{\text{num}}, f_{\rho\theta}^{\text{num}})$ is EC if

$$\left[\log \left(\frac{\rho}{\rho\theta} \right) \right] f_\rho^{\text{num}} - \left[\frac{\rho}{\rho\theta} \right] f_{\rho\theta}^{\text{num}} = 0. \quad (25)$$

We refer to (25) as the EC condition. Recalling that in the numerical TEC fluxes, the numerical density flux constituted a degree of freedom, we can employ this EC condition to derive two new numerical fluxes. The first is to use the density flux coming from (25) to obtain a flux which is TEC and EC, i.e.,

$$f_\rho^{\text{num}} = \frac{\left[\frac{\rho}{\rho\theta} \right]}{\left[\log \left(\frac{\rho}{\rho\theta} \right) \right]} f_{\rho\theta}^{\text{num}} = \{ \{ 1/\theta \} \}_{\log} f_{\rho\theta}^{\text{num}}. \quad (26)$$

However, this leads to an influence of the pressure in the density flux, which may lead to loss of positivity of pressure values [16]. The second choice is to use the potential temperature flux coming from (25), i.e.,

$$f_{\rho\theta}^{\text{num}} = \frac{\left[\log \left(\frac{\rho}{\rho\theta} \right) \right]}{\left[\frac{\rho}{\rho\theta} \right]} f_\rho = \frac{1}{\{ \{ 1/\theta \} \}_{\log}} f_\rho^{\text{num}}. \quad (27)$$

This numerical flux is EC by construction and presents a degree of freedom in the density flux. In summary, we consider the numerical fluxes

- **TEC Flux**

$$\begin{aligned} f_\rho^{\text{num}} &= \text{any consistent and symmetric flux of } \rho v, \\ f_{\rho v}^{\text{num}} &= f_\rho^{\text{num}} \{ \{ v \} \} + \{ \{ p \} \}, \\ f_{\rho\theta}^{\text{num}} &= \{ \{ \rho\theta \} \}_\gamma \{ \{ v \} \}, \end{aligned} \quad (28)$$

- **EC Flux**

$$\begin{aligned} f_\rho^{\text{num}} &= \text{any consistent and symmetric flux of } \rho v, \\ f_{\rho v}^{\text{num}} &= f_\rho^{\text{num}} \{ \{ v \} \} + \{ \{ p \} \}, \\ f_{\rho\theta}^{\text{num}} &= f_\rho^{\text{num}} \frac{1}{\{ \{ 1/\theta \} \}_{\log}} \end{aligned} \quad (29)$$

- **ETEC Flux (Entropy and Total Energy Conservative)**

$$\begin{aligned} f_\rho^{\text{num}} &= f_{\rho\theta}^{\text{num}} \{ \{ 1/\theta \} \}_{\log}, \\ f_{\rho v}^{\text{num}} &= f_\rho^{\text{num}} \{ \{ v \} \} + \{ \{ p \} \}, \\ f_{\rho\theta}^{\text{num}} &= \{ \{ \rho\theta \} \}_\gamma \{ \{ v \} \}. \end{aligned} \quad (30)$$

The first two fluxes allow for some degree of freedom in the choice of the density flux, which can be used to enforce additional structure-preserving properties. For sake of completeness, here we report the TEC flux in the x -direction for the 2D case with velocity $\mathbf{V} = (u, v)$:

$$\begin{aligned} f_\rho^{\text{num},x} &= \text{any consistent and symmetric flux of } \rho u, \\ f_{\rho u}^{\text{num},x} &= f_\rho^{\text{num},x} \{ \{ u \} \} + \{ \{ p \} \}, \\ f_{\rho v}^{\text{num},x} &= f_\rho^{\text{num},x} \{ \{ v \} \}, \\ f_{\rho\theta}^{\text{num},x} &= \{ \{ \rho\theta \} \}_\gamma \{ \{ u \} \}. \end{aligned} \quad (31)$$

The other fluxes are generalized analogously to multiple dimensions. In the next section, we further study and characterize the properties for all the fluxes.

3 Two-point flux structure-preserving properties of $(\rho, \rho v, \rho\theta)$

In this section we keep our analysis to the one-dimensional case

$$\partial_t \begin{pmatrix} \rho \\ \rho v \\ \rho\theta \end{pmatrix} + \partial_x \begin{pmatrix} \rho v \\ \rho v^2 + p \\ \rho\theta v \end{pmatrix} = \mathbf{0}, \quad (32)$$

and analyze in detail the different properties arising for the compressible Euler equations with the potential temperature and the derivation of our new fluxes (29), (28), and (30). First we recall the definition of fundamental and desirable properties of two-point numerical fluxes for the compressible Euler equations.

Definition 3.1 (Kinetic energy preservation [30, 36, 44–46]). A numerical flux $f^{\text{num}} = (f_{\varrho}^{\text{num}}, f_{\varrho v}^{\text{num}}, f_{\varrho\theta}^{\text{num}})$ is KEP if

$$f_{\varrho v}^{\text{num}} = \{\{v\}\} f_{\varrho}^{\text{num}} + \{\{p\}\}. \quad (33)$$

The pressure equilibrium preserving (PEP) property, given the relation between pressure and potential temperature, has to be reformulated in terms of the new conserved variables. Following [45], we introduce the following definition for the potential temperature.

Definition 3.2. A numerical flux $f^{\text{num}} = (f_{\varrho}^{\text{num}}, f_{\varrho v}^{\text{num}}, f_{\varrho\theta}^{\text{num}})$ is PEP if

$$f_{\varrho, v}^{\text{num}} = v f_{\varrho}^{\text{num}} + \text{const}(pv), \quad f_{\varrho\theta}^{\text{num}} = \text{const}(\varrho\theta, v), \quad (34)$$

provided that velocity v and pressure p are constant throughout the domain.

It is straightforward to prove that the TEC and ETEC numerical fluxes derived in the previous section are PEP. The above definition is motivated by the following

Lemma 3.3. *Pressure equilibrium, i.e., $p \equiv \text{const}$ and $v \equiv \text{const}$ is preserved by the FV semi-discretization if and only if the numerical flux is PEP.*

Proof. The pressure equation written in terms of the conserved variables $(\varrho, \varrho v, \varrho\theta)$ is

$$\partial_t p = \partial_t (K(\varrho\theta)^\gamma) = \gamma(\varrho\theta)^{\gamma-1} K \partial_t (\varrho\theta). \quad (35)$$

Recalling that $\partial_t (\varrho\theta) = -\partial_x (\varrho\theta v)$ and plugging into the previous equation,

$$\partial_t (p) = -\gamma K(\varrho\theta)^{\gamma-1} \partial_x (\varrho\theta v). \quad (36)$$

A semi-discretization of (36) leads to

$$\partial_t p_i = -\gamma K(\varrho\theta)_i^{\gamma-1} \frac{1}{\Delta x} (f_{\varrho\theta}^{\text{num}}(\mathbf{u}_{i+1}, \mathbf{u}_i) - f_{\varrho\theta}^{\text{num}}(\mathbf{u}_i, \mathbf{u}_{i-1})). \quad (37)$$

On the other hand, the semidiscrete evolution equation for the velocity is [45]

$$\varrho_i \partial_t v_i = \partial_t \varrho_i v_i = -\frac{1}{\Delta x} (f_{\varrho v}^{\text{num}}(\mathbf{u}_{i+1}, \mathbf{u}_i) - f_{\varrho v}^{\text{num}}(\mathbf{u}_i, \mathbf{u}_{i-1}) - v_i (f_{\varrho}^{\text{num}}(\mathbf{u}_{i+1}, \mathbf{u}_i) - f_{\varrho}^{\text{num}}(\mathbf{u}_i, \mathbf{u}_{i-1}))). \quad (38)$$

Thus, $\partial_t v_i = 0$ and $\partial_t p_i = 0$ if and only if (34) is satisfied. \square

3.1 Characterization of fluxes

Our first goal is to show that it is impossible to construct a numerical flux that is EC, TEC, KEP, PEP, and has no influence of the pressure in the density flux for the set of variables $(\varrho, \varrho v, \varrho\theta)$. In other words, when dealing with the potential temperature as primary invariant, the influence of the pressure term in the density flux cannot be avoided if TEC and EC are desired property for the numerical scheme, which can be formulated with the following

Theorem 3.4. *For the compressible Euler equations in potential temperature formulation (32), the ETEC flux (30) is EC, TEC, KEP and PEP. Moreover, it is the only numerical flux with these properties for $v \equiv \text{const}$.*

Remark. *Note that the numerical flux of Theorem 3.4 has a density flux influenced by the pressure, which may cause the density to assume negative values [16].*

To prove Theorem 3.4, we derive the necessary conditions for EC, TEC, and PEP.

Lemma 3.5. *For $p = \text{const}$, $v = \text{const}$, any consistent and symmetric numerical flux $f^{\text{num}} = (f_{\varrho}^{\text{num}}, f_{\varrho v}^{\text{num}}, f_{\varrho\theta}^{\text{num}})$ is TEC and KEP.*

Proof. If $p = \text{const}$, then $\varrho\theta = \text{const}$. Thus, the TEC condition becomes

$$-\frac{1}{2} \llbracket v^2 \rrbracket f_{\varrho}^{\text{num}} + \llbracket v \rrbracket f_{\varrho v}^{\text{num}} + \frac{\gamma K}{\gamma - 1} \llbracket (\varrho\theta)^{\gamma-1} \rrbracket f_{\varrho\theta}^{\text{num}} - K \llbracket (\varrho\theta)^\gamma v \rrbracket = 0, \quad (39)$$

and it is always satisfied for any numerical flux, given $p = \text{const}$ and $v = \text{const}$, since all the jumps vanish. \square

Lemma 3.6. For $p = \text{const}$, $v = \text{const}$, an EC and PEP numerical flux f^{num} satisfies

$$f_{\varrho\theta}^{\text{num}} = f_{\varrho}^{\text{num}} \{\{\varrho\}\}_{\log}^{-1} \varrho\theta. \quad (40)$$

Proof. It follows directly from the EC condition (25), when $p = \text{const}$. \square

Lemma 3.7. For $p = \text{const}$, $v = \text{const}$, an EC numerical flux that is also PEP or KEP must be of the form

$$\begin{cases} f_{\varrho}^{\text{num}} = \{\{\varrho\}\}_{\log} v \\ f_{\varrho v}^{\text{num}} = f_{\varrho}^{\text{num}} v + p \\ f_{\varrho\theta}^{\text{num}} = \varrho\theta v \end{cases} \quad (41)$$

Proof. Comparing the EC condition (25) with the PEP (34) or KEP (33), the density flux f_{ϱ}^{num} is independent of the potential temperature, hence

$$f_{\varrho}^{\text{num}} = \{\{\varrho\}\}_{\log} v, \quad (42)$$

and inserting the EC and KEP property the numerical flux has to be of the form (41). \square

Note that since for $p = \text{const}$ and $v = \text{const}$, TEC requires only a consistent and symmetric numerical flux, these numerical fluxes also satisfy the TEC condition (17).

Lemma 3.8. For $v = \text{const}$, an EC and PEP numerical flux for which the density flux does not depend on the pressure must be of the form

$$\begin{cases} f_{\varrho}^{\text{num}} = \{\{\varrho\}\}_{\log} v \\ f_{\varrho v}^{\text{num}} = f_{\varrho}^{\text{num}} v + \{\{p\}\} \\ f_{\varrho\theta}^{\text{num}} = \frac{\{\{\varrho\}\}_{\log}}{\{\{1/\theta\}\}_{\log}} v \end{cases} \quad (43)$$

Proof. Due to Lemma 3.7, the general form of the dependencies on ϱ for $p \equiv \text{const}$ is already determined. The remaining degree of freedom for non-constant pressure p can be described by two functions $\varphi_{1,2}$, resulting in the numerical fluxes

$$\begin{cases} f_{\varrho}^{\text{num}} = \{\{\varrho\}\}_{\log} v \\ f_{\varrho v}^{\text{num}} = f_{\varrho}^{\text{num}} v + \varphi_1(\varrho_{\pm}, p_{\pm}) \\ f_{\varrho\theta}^{\text{num}} = \varphi_2(\varrho_{\pm}, \varrho\theta_{\pm}) v \end{cases} \quad (44)$$

where $\varphi_1(\varrho_{\pm}, p_{\pm})$ and $\varphi_2(\varrho_{\pm}, \varrho\theta_{\pm})$ are some kind of mean values depending on $\varrho_{\pm}, p_{\pm}, \varrho\theta_{\pm}$ such that

$$\begin{aligned} \forall \varrho_{\pm}, p > 0: \quad \varphi_1(\varrho_+, \varrho_-, p, p) &= p, \\ \forall \varrho_{\pm}, \varrho\theta > 0: \quad \varphi_2(\varrho_+, \varrho_-, \varrho\theta, \varrho\theta) &= \varrho\theta. \end{aligned} \quad (45)$$

For the KEP condition, $\varphi_1(\varrho_{\pm}, p) = \{\{p\}\}$. Substituting the fluxes (44) into the EC condition (25),

$$\varphi_2(\varrho_{\pm}, \varrho\theta_{\pm}) = \frac{\{\{\varrho\}\}_{\log}}{\{\{1/\theta\}\}_{\log}}, \quad (46)$$

which satisfies the condition (45). \square

Lemma 3.9. For $v = \text{const}$, a TEC flux for the potential temperature must be of the form

$$f_{\varrho\theta} = \{\{\varrho\theta\}\}_{\gamma} v. \quad (47)$$

Proof. The potential temperature numerical flux can be described for constant velocities as

$$f_{\varrho\theta} = \varphi_2(\varrho_{\pm}, \varrho\theta_{\pm}) v, \quad (48)$$

where φ_2 is some kind of mean values depending on $\varrho_{\pm}, \varrho\theta_{\pm}$ such that

$$\forall \varrho_{\pm}, \varrho\theta > 0: \quad \varphi_2(\varrho_+, \varrho_-, \varrho\theta, \varrho\theta) = \varrho\theta. \quad (49)$$

The TEC condition (17) for $v = \text{const}$ becomes

$$\frac{\gamma K}{\gamma - 1} [(\varrho\theta)^{\gamma-1}] f_{\varrho\theta} - K [(\varrho\theta)^{\gamma}] v = 0, \quad (50)$$

which results in the final form (47). \square

Thus, for $v = \text{const}$ a numerical flux that is PEP, EC, TEC, and has a density flux that does not depend on the pressure cannot be constructed, since in the relation

$$\{\{\varrho\theta\}\}_\gamma = \frac{\{\{\varrho\}\}_{\log}}{\{\{1/\theta\}\}_{\log}}, \quad (51)$$

for a fixed γ , there exists at least one tuple $(\varrho_\pm, \theta_\pm)$ such that the relation above is not satisfied. We showed that a numerical flux that is EC, PEP, TEC, and does not have the influence of the pressure in the density flux cannot exist for $v = \text{const}$. Thus, we are ready to introduce the dependence of the pressure in the density flux.

Lemma 3.10. *For $v = \text{const}$, a numerical flux that is PEP, EC, and TEC must be of the form*

$$\begin{cases} f_\varrho^{\text{num}} = \{\{\varrho\}\}_\gamma \{\{1/\theta\}\}_{\log} v \\ f_{\varrho v}^{\text{num}} = f_\varrho v + \{\{p\}\} \\ f_{\varrho\theta}^{\text{num}} = \{\{\varrho\}\}_\gamma v \end{cases} \quad (52)$$

with the influence of the pressure in the numerical density flux.

Proof. The form of the potential temperature flux has already been determined by Lemma 3.9. The remaining dependencies in the density and momentum flux can be again described by the functions $\varphi_{1,2}$ resulting in the numerical fluxes

$$\begin{cases} f_\varrho^{\text{num}} = \varphi_2(\varrho_\pm, \varrho\theta_\pm)v \\ f_{\varrho v}^{\text{num}} = f_\varrho^{\text{num}}v + \varphi_1(\varrho_\pm, p_\pm) \\ f_{\varrho\theta}^{\text{num}} = \frac{\gamma}{\gamma - 1} \frac{\llbracket(\varrho\theta)^\gamma\rrbracket}{\llbracket(\varrho\theta)^{\gamma-1}\rrbracket}v \end{cases} \quad (53)$$

where $\varphi_1(\varrho_\pm, p_\pm)$ and $\varphi_2(\varrho_\pm, \varrho\theta_\pm)$ are some kind of mean values depending on $\varrho_\pm, p_\pm, \varrho\theta_\pm$ such that

$$\begin{aligned} \forall \varrho_\pm, p > 0: \quad \varphi_1(\varrho_+, \varrho_-, p, p) &= p, \\ \forall \varrho_\pm, \varrho\theta > 0: \quad \varphi_2(\varrho_+, \varrho_-, \varrho\theta, \varrho\theta) &= \varrho. \end{aligned} \quad (54)$$

The final form (52) is given by the substituting the numerical fluxes (53) into the conditions EC (25) and PEP (34). \square

We can now prove Theorem 3.4.

Proof of Theorem 3.4. The EC (25) and TEC (17) conditions are verified by substituting the numerical fluxes into (25) and (17). The KEP (33) property is verified by construction and the characterization for $v = \text{const}$ has been proven in Lemma 3.10. \square

The characterization of the numerical fluxes for the compressible Euler equations with potential temperature as first invariant has been completed. The numerical fluxes are characterized by the influence of the pressure in the density flux, which is necessary to satisfy the EC, TEC, and PEP properties. In the following lemma we show the characterization for $p = \text{const}$.

Lemma 3.11. *For fixed $p = \text{const}$, a (symmetric) EC, TEC, KEP, and PEP numerical flux must be of the form*

$$\begin{cases} f_\varrho^{\text{num}} = \{\{\varrho\}\}_\gamma \{\{v\}\} + \chi(\varrho_\pm, v_\pm) \\ f_{\varrho v}^{\text{num}} = f_\varrho^{\text{num}} \{\{v\}\} + \{\{p\}\} + \{\{v\}\} \chi(\varrho_\pm, v_\pm) \\ f_{\varrho\theta}^{\text{num}} = \varrho\theta \{\{v\}\} + \frac{\varrho\theta}{\{\{\varrho\}\}_{\log}} \chi(\varrho_\pm, v_\pm) \end{cases} \quad (55)$$

where χ is a function depending on ϱ_\pm, v_\pm such that $\forall \varrho_\pm, v: \chi(\varrho_+, \varrho_-, v, v) = 0$.

Proof. The proof is analogous to the one in [45]. Indeed, due to consistency, a numerical flux can always be written as the sum of a given numerical flux and a perturbation χ that is consistent with zero. Therefore, we add the perturbation χ to the numerical fluxes from Theorem 3.4, considering that $p = \text{const}$, so that

$$\begin{cases} f_\varrho^{\text{num}} = \{\{\varrho\}\}_\gamma \{\{v\}\} + \chi_\varrho(\varrho_\pm, v_\pm) \\ f_{\varrho v}^{\text{num}} = f_\varrho^{\text{num}} \{\{v\}\} + \{\{p\}\} + \{\{v\}\} \chi_{\varrho v}(\varrho_\pm, v_\pm) \\ f_{\varrho\theta}^{\text{num}} = \varrho\theta \{\{v\}\} + \chi_{\varrho\theta}(\varrho_\pm, v_\pm) \end{cases} \quad (56)$$

where $\forall \varrho, v: \chi_\varrho(\varrho_+, \varrho_-, v, v) = 0, \chi_{\varrho v}(\varrho_+, \varrho_-, v, v) = 0$ and $X_{\varrho\theta}(\varrho_+, \varrho_-, v, v) = 0$. The perturbation χ is then chosen such that the EC, TEC, KEP, and PEP conditions are satisfied. The KEP property leads to the condition $\chi_{\varrho v} = \{\{v\}\} \chi_\varrho$. The TEC condition (17) for $p = \text{const}$ yields

$$-\frac{1}{2} \left[\frac{m^2}{\varrho^2} \right] \left(\frac{\gamma-1}{\gamma} \frac{[\varrho^\gamma]}{[\varrho^{\gamma-1}]} \{\{v\}\} + \chi_\varrho(\varrho_\pm, v_\pm) \right) + \left[\frac{m}{\varrho} \right] \left(\frac{\gamma-1}{\gamma} \frac{[\varrho^\gamma]}{[\varrho^{\gamma-1}]} \{\{v\}\}^2 + p + \chi_\varrho(\varrho_\pm, v_\pm) \{\{v\}\} \right) - p [\{v\}] = 0, \quad (57)$$

which is always satisfied, for any perturbation χ_ϱ . The EC condition (25) leads to

$$\chi_{\varrho\theta} = \frac{\varrho\theta}{\{\{\varrho\}\}_{\log}} \chi_\varrho, \quad (58)$$

which is satisfied for any perturbation χ_ϱ that satisfies the condition $\forall \varrho, v: \chi_\varrho(\varrho_+, \varrho_-, v, v) = 0$. The PEP is satisfied if and only if the perturbation term is such that $\forall \varrho, v: \chi_\varrho(\varrho_+, \varrho_-, v, v) = 0$. \square

The extension of the numerical fluxes (56) to an arbitrary non-constant pressure is straightforward and due to the form of the fluxes in Theorem 3.4, the numerical flux is unique also for general velocities.

3.2 On the pressure positivity for $(\varrho, \varrho v, \varrho\theta)$

Density and pressure must be positive to avoid nonphysical numerical solutions and eventually instabilities. The numerical fluxes should preserve this property when an explicit Euler time marching method is applied to a first-order FV method. This is a well-known and important property, since SSP Runge-Kutta methods can be written as a convex combination of Euler steps method [27]. Therefore, given the convex set of admissible states

$$G = \{\mathbf{u} = (\varrho, \varrho v, \varrho\theta) \mid \varrho > 0, p = K(\varrho\theta)^\gamma > 0\}, \quad (59)$$

positivity of density and pressure is inherited by any convex combination of Euler steps, as soon as it is preserved by the internal Euler steps. Note that the density positivity remains unchanged with respect to the results already described in [43]. However, the advantage of the potential temperature formulation results in a straightforward way to preserve the pressure positivity.

Corollary 3.12. *If the numerical potential temperature flux $f_{\varrho\theta}^{\text{num}} = \{\{\varrho\theta\}\}_\gamma \{\{v\}\} - \frac{\lambda}{2} [\varrho\theta]$ is used with $\lambda \geq \max\{|v_i|, |v_{i+1}|\}$, the first-order FV scheme preserves the non-negativity of the pressure ϱ under the CFL condition*

$$\Delta t \leq \frac{\Delta x}{2\lambda}. \quad (60)$$

Proof. The mean appearing in the flux is given by the integral for $t = 2 - \gamma$ (see [12])

$$f(t) = \frac{\int_a^b x^{t+1} dx}{\int_a^b x^t dx}. \quad (61)$$

Thus,

$$f(2 - \gamma) = \{\{\varrho\theta\}\}_\gamma, \quad (62)$$

and due to the monotonicity of f , we have

$$f(2 - \gamma) = \{\{\varrho\theta\}\}_\gamma \leq f(0) = \{\{\varrho\theta\}\}. \quad (63)$$

Hence, this mean satisfies the conditions of Theorem 6.1 in [43] and the flux preserves the positivity of the potential temperature. Pressure positivity follows, since

$$p_i^{n+1} = K(\varrho\theta)_i^{n+1} \geq 0 \quad \forall n \in \mathbb{N}. \quad (64)$$

\square

In Table 1 we provide a summary overview of the properties of the derived fluxes. It is important to emphasize that the PEP property can only be achieved for an EC flux if the density flux is constructed with logarithmic mean, thereby reducing the degree of freedom in its derivation. On the other hand, a TEC flux does not present this limitation.

Table 1: Properties and conserved variables for the different derived numerical fluxes. ✓: variable conserved or property satisfied. ✗: variable not conserved or property is not satisfied. $\bar{\varrho} = \{\{\varrho\}\}_{\log}$: property satisfied only if the density in the f_ϱ flux is discretized with a logarithmic mean.

Conserved Variables and Properties	Numerical Fluxes		
	EC (29)	TEC (28)	ETEC (30)
ρE	✗	✓	✓
ρs	✓	✗	✓
$\rho \theta$	✓	✓	✓
KEP	✓	✓	✓
PEP	$\bar{\varrho} = \{\{\varrho\}\}_{\log}$	✓	✓
No Pressure Term in the Density Flux f_θ	✓	✓	✗

4 On the conservation properties in presence of a geopotential term

To include gravity effects, typically a source term with a geopotential term $\phi = \phi(x)$ is added to the right-hand side of the compressible Euler equations, as in Eqs (1) and (2). The momentum and the total energy are not conserved anymore and other invariants and properties play a significant role in geophysical flows. Souza et al. [57] have developed a kinetic and potential energy preserving (KPEP) numerical flux with the total energy as conserved variable using the Kennedy-Gruber flux [31] for the conservative part of the Euler equations. In this section, we extend the KPEP property introduced in [57]. We first present a general condition for KPEP fluxes within the FV framework. Furthermore, we introduce the condition for total energy conservation in the presence of gravity, considering two sets of conserved variables: $(\varrho, \varrho v, \varrho E)$ and $(\varrho, \varrho v, \varrho \theta)$. To do that, we employ a non-conservative discretization of the source terms.

4.1 On the kinetic and total energy

In presence of gravity source terms given by a generic geopotential ϕ , the compressible Euler equations in 1D read

$$\partial_t \begin{pmatrix} \varrho \\ \varrho v \\ \varrho E \end{pmatrix} + \partial_x \begin{pmatrix} \varrho v \\ \varrho v^2 + p \\ (\varrho E + p)v \end{pmatrix} = \begin{pmatrix} 0 \\ -\varrho \partial_x \phi \\ -\varrho v \partial_x \phi \end{pmatrix} \quad (65)$$

for $(\varrho, \varrho v, \varrho E)$ as conserved variables; for the potential temperature formulation, we have

$$\partial_t \begin{pmatrix} \varrho \\ \varrho v \\ \varrho \theta \end{pmatrix} + \partial_x \begin{pmatrix} \varrho v \\ \varrho v^2 + p \\ \varrho \theta v \end{pmatrix} = \begin{pmatrix} 0 \\ -\varrho \partial_x \phi \\ 0 \end{pmatrix}. \quad (66)$$

The FV method in presence of a source term is typically written as

$$\partial_t \mathbf{u}_i + \frac{1}{\Delta x} \left(\mathbf{f}^{\text{num}}(\mathbf{u}_i, \mathbf{u}_{i+1}) - \mathbf{f}^{\text{num}}(\mathbf{u}_{i-1}, \mathbf{u}_i) \right) = \mathbf{S}_i. \quad (67)$$

We seek for a particular discretization of the source term \mathbf{S}_i and conditions such that for both semi-discretization the KPEP and TEC property are satisfied, where the total energy for the systems (65) and (66) is $U = \varrho E + \varrho \phi$, which is a conserved quantity. In particular, following the work of [20, 47], we introduce the general form for the discretization of source terms

$$S_i^{\varrho v} = \frac{S_{i+1/2}^{\varrho v} + S_{i-1/2}^{\varrho v}}{2\Delta x} = \frac{\bar{\varrho}_{i+1/2} \llbracket \phi \rrbracket_{i+1/2} + \bar{\varrho}_{i-1/2} \llbracket \phi \rrbracket_{i-1/2}}{2\Delta x}, \quad (68)$$

$$S_i^{\varrho E} = \frac{S_{i+1/2}^{\varrho E} + S_{i-1/2}^{\varrho E}}{2\Delta x} = \frac{\bar{v}_{i+1/2} \bar{\varrho}_{i+1/2} \llbracket \phi \rrbracket_{i+1/2} + \bar{v}_{i-1/2} \bar{\varrho}_{i-1/2} \llbracket \phi \rrbracket_{i-1/2}}{2\Delta x}, \quad (69)$$

where $\bar{\varrho}_{i+1/2}$ and $\bar{v}_{i+1/2}$ are consistent mean values, such that

$$\begin{aligned}\forall \varrho_{i+1} = \varrho = \varrho_i > 0: \quad \bar{\varrho}_{i+1/2} &= \varrho, \\ \forall v_{i+1} = v = v_i: \quad \bar{v}_{i+1/2} &= v.\end{aligned}\tag{70}$$

We therefore investigate the necessary conditions for ensuring KPEP and TEC property.

Lemma 4.1. *Given the set of variables $(\varrho, \varrho v, \varrho \theta)$, a numerical flux $(f_\varrho^{\text{num}}, f_{\varrho v}^{\text{num}}, f_{\varrho \theta}^{\text{num}})$, the source term S^{ev} and the corresponding FV method (7) are TEC if*

(i) *the density flux and the source term are of the form*

$$f_\varrho^{\text{num}} = \bar{\varrho} \{\{v\}\}, \quad S^{ev} = \bar{\varrho} \llbracket \phi \rrbracket\tag{71}$$

(ii) *and the numerical flux $(f_\varrho^{\text{num}}, f_{\varrho v}^{\text{num}}, f_{\varrho \theta}^{\text{num}})$ is of the form (28).*

Proof. The proof requires the contraction of the right-hand side in entropy space. Therefore, we consider the total energy

$$U = \varrho E + \varrho \phi = \frac{p}{\gamma - 1} + \frac{1}{2} \frac{m^2}{\varrho} + \varrho \phi.\tag{72}$$

The entropy variables for the new entropy functional U can be written as

$$\boldsymbol{\omega} = \boldsymbol{\omega}_{\rho E} + \boldsymbol{\omega}_\phi = \begin{pmatrix} -\frac{1}{2} \frac{m^2}{\varrho^2} \\ \frac{m}{\varrho} \\ -\frac{\gamma}{\gamma-1} K(\varrho \theta)^{\gamma-1} \end{pmatrix} + \begin{pmatrix} \phi \\ 0 \\ 0 \end{pmatrix}.\tag{73}$$

Hence, we can use this linear relation between the total energy including the potential. Therefore, performing a left multiplication of (67) by the entropy variables (73) yields

$$\frac{dU_i}{dt} = -\frac{1}{\Delta x} \left(\langle \boldsymbol{\omega}_i, \mathbf{f}_{i+1/2} \rangle - \langle \boldsymbol{\omega}_i, \mathbf{f}_{i-1/2} \rangle \right) - \langle \boldsymbol{\omega}_i, \mathbf{S}_i \rangle,\tag{74}$$

where we introduced the abbreviation $\mathbf{f}_{i+1/2} = f^{\text{num}}(\mathbf{u}_i, \mathbf{u}_{i+1})$. By expressing the first two terms as $\boldsymbol{\omega}_i = \{\{\boldsymbol{\omega}\}\}_{i\pm 1/2} \mp \frac{1}{2} \llbracket \boldsymbol{\omega} \rrbracket_{i\pm 1/2}$, we obtain

$$\begin{aligned}\frac{dU_i}{dt} &= -\frac{1}{\Delta x} \left(\langle \{\{\boldsymbol{\omega}\}\}_{i+1/2}, \mathbf{f}_{i+1/2} \rangle - \frac{1}{2} \langle \llbracket \boldsymbol{\omega} \rrbracket_{i+1/2}, \mathbf{f}_{i+1/2} \rangle \right) \\ &\quad - \frac{1}{\Delta x} \left(\langle \{\{\boldsymbol{\omega}\}\}_{i-1/2}, \mathbf{f}_{i-1/2} \rangle + \frac{1}{2} \langle \llbracket \boldsymbol{\omega} \rrbracket_{i-1/2}, \mathbf{f}_{i-1/2} \rangle \right) - \langle \boldsymbol{\omega}_i, \mathbf{S}_i \rangle.\end{aligned}\tag{75}$$

Therefore, we can split the different contributions and employing the TEC definition and the definition of the source term, we are left with

$$\frac{dU_i}{dt} = -\frac{1}{\Delta x} (F_{i+1/2} - F_{i-1/2}) - \frac{\phi_i}{\Delta x} (f_{i+1/2}^e - f_{i-1/2}^e) - v_i \frac{\bar{\varrho}_{i+1/2} \llbracket \phi \rrbracket_{i+1/2} + \bar{\varrho}_{i-1/2} \llbracket \phi \rrbracket_{i-1/2}}{2\Delta x},\tag{76}$$

where $F_{i+1/2}$ is the conservative and symmetric total energy flux. Following a similar argument as before,

$$\begin{aligned}\frac{dU_i}{dt} &= -\frac{1}{\Delta x} (F_{i+1/2} - F_{i-1/2}) - \frac{1}{\Delta x} (f_{i+1/2}^e \{\{\phi\}\}_{i+1/2} - f_{i-1/2}^e \{\{\phi\}\}_{i-1/2}) + \\ &\quad + \frac{\bar{\varrho}_{i+1/2} \llbracket \phi \rrbracket_{i+1/2} \llbracket v \rrbracket_{i+1/2} - \bar{\varrho}_{i-1/2} \llbracket \phi \rrbracket_{i-1/2} \llbracket u \rrbracket_{i-1/2}}{4\Delta x} + \\ &\quad + \frac{\llbracket \phi \rrbracket_{i+1/2} f_{i+1/2}^e + \llbracket \phi \rrbracket_{i-1/2} f_{i-1/2}^e}{2\Delta x} - \frac{\bar{\varrho}_{i+1/2} \llbracket \phi \rrbracket_{i+1/2} \{\{v\}\}_{i+1/2} + \bar{\varrho}_{i-1/2} \llbracket \phi \rrbracket_{i-1/2} \{\{v\}\}_{i-1/2}}{2\Delta x}.\end{aligned}\tag{77}$$

If $f_{i+1/2}^e = \bar{\varrho}_{i+1/2} \{\{v\}\}_{i+1/2}$ then the last two terms vanish

$$\begin{aligned}\frac{dU_i}{dt} &= -\frac{1}{\Delta x} (F_{i+1/2} - F_{i-1/2}) - \frac{1}{\Delta x} (f_{i+1/2}^e \{\{\phi\}\}_{i+1/2} - f_{i-1/2}^e \{\{\phi\}\}_{i-1/2}) \\ &\quad + \frac{\bar{\varrho}_{i+1/2} \llbracket \phi \rrbracket_{i+1/2} \llbracket v \rrbracket_{i+1/2} - \bar{\varrho}_{i-1/2} \llbracket \phi \rrbracket_{i-1/2} \llbracket v \rrbracket_{i-1/2}}{4\Delta x},\end{aligned}\tag{78}$$

which can be written in a conservative form as

$$\frac{dU_i}{dt} = -\frac{1}{\Delta x}(H_{i+1/2} - H_{i-1/2}), \quad (79)$$

where

$$H_{i+1/2} = F_{i+1/2} + f_{i+1/2}^{\rho} \{\{\phi\}\}_{i+1/2} - \frac{\bar{\rho}_{i+1/2}}{4} [\phi]_{i+1/2} [v]_{i+1/2}. \quad (80)$$

Note that for the set of conserved variables with the potential temperature we had to impose the TEC flux derived in the previous section. That is not required when working with $(\rho, \rho v, \rho E)$ as primary variables, since ρE is a first invariant when $\phi = 0$.

Lemma 4.2. *Given the set of conserved variables $(\rho, \rho v, \rho E)$, a numerical flux $(f_{\rho}^{\text{num}}, f_{\rho v}^{\text{num}}, f_{\rho E}^{\text{num}})$, the source terms S^{ev} , $S^{\rho E}$ and the corresponding FV method (7) are TEC if the density flux and the source terms are of the form*

$$f_{\rho}^{\text{num}} = \bar{\rho} \{\{v\}\}, \quad S^{ev} = \bar{\rho} [\phi], \quad S^{\rho E} = f_{\rho}^{\text{num}} [\phi]. \quad (81)$$

Proof. A semi-discretization of the total energy starting with the given set of conserved variables can be written as

$$\partial_t(\rho_i E_i + \phi_i \rho_i) = \partial_t(\rho_i E_i) + \phi_i \partial_t(\rho_i), \quad (82)$$

since the geopotential depends only on the space coordinates. Following the same steps as shown before, and considering $f_{i+1/2}^{\rho} = \bar{v}_{i+1/2} \bar{\rho}_{i+1/2}$ we obtain

$$\begin{aligned} \frac{d(\rho_i E_i + \phi_i \rho_i)}{dt} &= -\frac{1}{\Delta x}(f_{i+1/2}^{\rho E} - f_{i-1/2}^{\rho E}) - \frac{\phi_i}{\Delta x}(f_{i+1/2}^{\rho} - f_{i-1/2}^{\rho}) \\ &\quad - \frac{\bar{v}_{i+1/2} \bar{\rho}_{i+1/2} [\phi]_{i+1/2} + \bar{v}_{i-1/2} \bar{\rho}_{i-1/2} [\phi]_{i-1/2}}{2\Delta x}, \end{aligned} \quad (83)$$

which can be further developed into

$$\begin{aligned} \frac{d(\rho_i E_i + \phi_i \rho_i)}{dt} &= -\frac{1}{\Delta x}(f_{i+1/2}^{\rho E} - f_{i-1/2}^{\rho E}) - \frac{1}{\Delta x}(f_{i+1/2}^{\rho} \{\{\phi\}\}_{i+1/2} - f_{i-1/2}^{\rho} \{\{\phi\}\}_{i-1/2}) \\ &\quad + \frac{[\phi]_{i+1/2} f_{i+1/2}^{\rho} + [\phi]_{i-1/2} f_{i-1/2}^{\rho}}{2\Delta x} - \frac{\bar{v}_{i+1/2} \bar{\rho}_{i+1/2} [\phi]_{i+1/2} + \bar{v}_{i-1/2} \bar{\rho}_{i-1/2} [\phi]_{i-1/2}}{2\Delta x}. \end{aligned} \quad (84)$$

The last two terms vanishes if $f_{i+1/2}^{\rho} = \bar{v}_{i+1/2} \bar{\rho}_{i+1/2}$; its conservative form is

$$\frac{d}{dt}(\rho_i E_i + \phi_i \rho_i) = -\frac{1}{\Delta x}(H_{i+1/2} - H_{i-1/2}), \quad (85)$$

where H is the numerical flux of the total energy

$$H_{i+1/2} = f_{i+1/2}^{\rho E} + f_{i+1/2}^{\rho} \{\{\phi\}\}_{i+1/2}. \quad (86)$$

Following the same approach as above, we investigate the condition for the numerical fluxes to achieve kinetic and potential energy preserving (KPEP) property. Since the momentum equation and the KEP property is not influenced by the set of variables, we can formulate a single lemma, that accounts for both.

Lemma 4.3. *Given the set of conserved variables $(\rho, \rho v, \rho E)$ or $(\rho, \rho v, \rho \theta)$, a numerical flux $(f_{\rho}^{\text{num}}, f_{\rho v}^{\text{num}}, f_{\rho E}^{\text{num}})$ or $(f_{\rho}^{\text{num}}, f_{\rho v}^{\text{num}}, f_{\rho \theta}^{\text{num}})$, a source term S^{ev} and the corresponding FV method (7) are KPEP if*

(i) *the density flux and the source term are of the form*

$$f_{\rho}^{\text{num}} = \bar{\rho} \{\{v\}\}, \quad S^{ev} = \bar{\rho} [\phi] \quad (87)$$

(ii) *and the numerical flux is KEP.*

Proof. First we note that

$$\partial_t \left(\frac{1}{2} k + \rho \phi \right) = v \partial_t(\rho v) - \frac{v^2}{2} \partial_t \rho + \phi \partial_t \rho = -\partial_x \left(v \left(\frac{1}{2} \rho v^2 + p + \rho \phi \right) \right) + p \partial_x v. \quad (88)$$

A semi-discretization leads to

$$\partial_t \left(\frac{1}{2} \rho_i v_i^2 + \rho_i \phi_i \right) = -v_i \frac{f_{i+1/2}^{\rho v} - f_{i-1/2}^{\rho v}}{\Delta x} + \frac{v_i^2}{2} \frac{f_{i+1/2}^{\rho} - f_{i-1/2}^{\rho}}{\Delta x} - v_i S_i^{ev} - \phi_i \frac{f_{i+1/2}^{\rho} - f_{i-1/2}^{\rho}}{\Delta x}. \quad (89)$$

If $f_{\rho v}^{\text{num}}$ is KEP, this proof reduces to finding a condition that results in a conservative form for the last two terms. This has already been done in the previous lemmas, leading to the same condition. \square

4.2 Well-balanced schemes

Steady states are particular solutions of the compressible Euler equations. In this section, we show how to construct well-balanced schemes by employing the same non-conservative product discretization as in the previous section. In particular, in presence of a potential the scheme should be able to mimic at a discrete level the hydrostatic balance of the Euler equations, i.e.,

$$\nabla p = -\varrho \nabla \phi. \quad (90)$$

The steady background state is typically prescribed either with an isothermal or constant potential temperature state, where then perturbations are added. Waruszewski et al. [63] derived a well-balanced scheme with isothermal background state for DG methods using a generalization of flux differencing for numerical fluxes in fluctuation form. Based on their results, here we show that this also applies for our FV methods and we present a well-balanced scheme for a constant potential temperature background state.

The only equation which plays a role in the well-balanced scheme is the momentum. Thus, independently of the last closure equation, (ϱE or $\varrho \theta$, or yet more general), these results are satisfied as long as the momentum ϱv is employed as primary invariant.

Lemma 4.4. *A source term S^{ev} preserves the hydrostatic balance prescribed by a constant background temperature T of the compressible Euler equations if the source term is of the form*

$$S^{ev} = \{\{\varrho\}\}_{\log} \llbracket \phi \rrbracket, \quad (91)$$

and the pressure term is discretized as $\{\{p\}\}$.

Proof. Presenting the idea in 1D, we consider

$$\partial_x p = -\varrho \partial_x \phi. \quad (92)$$

A solution of (92) must be of the form

$$p = p_0 e^{-\frac{\phi}{RT}} \quad \text{and} \quad \varrho = \varrho_0 e^{-\frac{\phi}{RT}} = \frac{p_0}{RT} e^{-\frac{\phi}{RT}}, \quad (93)$$

where $p_0 = p(x=0)$ and $\varrho_0 = \varrho(x=0)$. The semi-discretization (67) reduces to

$$\frac{\{\{p\}\}^+ - \{\{p\}\}^-}{\Delta x} + \frac{\{\{\varrho\}\}_{\log} \llbracket \phi \rrbracket^+ + \{\{\varrho\}\}_{\log} \llbracket \phi \rrbracket^-}{2\Delta x} = 0, \quad (94)$$

where we introduced the abbreviation $\{\{a\}\}^\pm = \{\{a\}\}_{i\pm 1/2}$. Inserting (93) results in

$$RT \frac{\{\{\varrho\}\}^+ - \{\{\varrho\}\}^-}{\Delta x} - RT \frac{\llbracket \phi \rrbracket^+ + \llbracket \phi \rrbracket^-}{2\Delta x} = 0, \quad (95)$$

which is always satisfied $\forall \varrho^\pm$. \square

For constant potential temperature background state, we consider the hydrostatic balance explicitly expressed in terms of the variable $\varrho \theta$, namely in 1D

$$K \partial_x (\varrho \theta)^\gamma = -\varrho \partial_x \phi. \quad (96)$$

If no perturbations in θ are present, i.e., $\theta = \text{const}$, the relation simplifies to

$$K \theta^\gamma \partial_x \varrho^\gamma = -\varrho \partial_x \phi, \quad (97)$$

and a closed form solution is of the form

$$\frac{1}{\gamma-1} \left(\varrho^{\gamma-1} - \varrho_0^{\gamma-1} \right) = -\frac{1}{K \gamma \theta^\gamma} (\phi - \phi_0), \quad (98)$$

where $\varrho_0 = \varrho(x=0)$ and $\phi_0 = \phi(x=0)$. At this point we can prove the following lemma.

Lemma 4.5. *A source term S^{ev} preserves the hydrostatic balance prescribed by a constant background potential temperature θ of the compressible Euler equations if the source term is of the form*

$$S^{ev} = \{\{\varrho\}\}_\gamma \llbracket \phi \rrbracket, \quad (99)$$

and the pressure term is discretized as $\{\{p\}\}$.

Proof. The semi-discretization (67) at the steady state reads

$$\frac{\{\{p\}\}^+ - \{\{p\}\}^-}{\Delta x} + \frac{\frac{\gamma-1}{\gamma} \frac{[\varrho^\gamma]}{[\varrho^{\gamma-1}]} [\phi]^+ + \frac{\gamma-1}{\gamma} \frac{[\varrho^\gamma]}{[\varrho^{\gamma-1}]} [\phi]^-}{2\Delta x} = 0. \quad (100)$$

Using the steady state solution (98), we can write the source term as

$$S = \frac{\gamma-1}{\gamma} \frac{[\varrho^\gamma]}{[\varrho^{\gamma-1}]} [\phi] = -K\theta^\gamma [\varrho^\gamma], \quad (101)$$

and consequently the semi-discretization reduces to

$$K\theta^\gamma \frac{\{\{\varrho^\gamma\}\}^+ - \{\{\varrho^\gamma\}\}^-}{\Delta x} - K\theta^\gamma \frac{[\varrho^\gamma]^+ + [\varrho^\gamma]^-}{2\Delta x} = 0, \quad (102)$$

which is always identically zero $\forall \varrho^\pm$, for the general property that $a_i = \{\{a\}\}^\pm \mp \frac{[a]^\pm}{2}$. \square

In Tables 2 and 3 we summarize the properties of the different numerical fluxes derived in this section. Note that an EC numerical flux for $(\varrho, \varrho v, \varrho E)$ cannot be TEC, KPEP and preserve hydrostatic balance for $\theta = \text{const}$ due to $f_\varrho^{\text{num}} = \{\{\varrho\}\}_{\log} \{\{v\}\}$. On the other hand, for $\varrho\theta$ you can always at least satisfy two conditions among TEC, KPEP and well-balancedness for $\theta = \text{const}$ or $T = \text{const}$.

Table 2: Properties and conserved variables for the different derived numerical fluxes. \checkmark : variable conserved or property satisfied. \times : variable not conserved or property not satisfied.

$S^{\varrho v} = \{\{\varrho\}\}_{\log} [\phi]$ Conserved Variables and Properties	Numerical Fluxes		
	EC	TEC	ETEC
KPEP	\checkmark	\checkmark	\times
TEC (including potential)	\times	\checkmark	\times
Hydrostatic Balance $T = \text{const}$	\checkmark	\checkmark	\checkmark
Hydrostatic Balance $\theta = \text{const}$	\times	\times	\times

Table 3: Properties and conserved variables for the different derived numerical fluxes. \checkmark : variable conserved or property satisfied. \times : variable not conserved or property not satisfied.

$S^{\varrho v} = \{\{\varrho\}\}_\gamma [\phi]$ Conserved Variables and Properties	Numerical Fluxes		
	EC	TEC	ETEC
KPEP	\checkmark	\checkmark	\times
TEC	\times	\checkmark	\times
Hydrostatic Balance $T = \text{const}$	\times	\times	\times
Hydrostatic Balance $\theta = \text{const}$	\checkmark	\checkmark	\checkmark

5 Entropy-conservative DGSEM discretization

In this section we extend all the previous properties to DGSEM. To obtain an entropy-stable DGSEM discretization of a conservation law

$$\partial_t \mathbf{u} + \partial_x \mathbf{f}(\mathbf{u}) = \mathbf{0}, \quad (103)$$

the computational domain is divided into non-overlapping elements. Within each element, the solution is approximated by Lagrange polynomials of degree N defined on the Lobatto-Gauss-Legendre (LGL) nodes. These basis functions are continuous inside each element but may be discontinuous across element boundaries. Such discontinuities are resolved with the introduction of two-point numerical fluxes.

The discrete scheme is obtained by multiplying the governing equation by test functions of degree N , integrating by parts on each element, and evaluating the resulting integrals using an LGL quadrature rule with $N + 1$ nodes on the reference interval $\xi \in [-1, 1]$. This procedure leads to the semi-discrete formulation

$$J\omega_i \dot{\mathbf{u}}_i(t) + (\mathbf{f}_{(N,R)}^* - \mathbf{f}(\mathbf{u}_i(t)))\delta_{iN} - (\mathbf{f}_{(0,L)}^* - \mathbf{f}(\mathbf{u}_i(t)))\delta_{i0} + 2 \sum_{j=0}^N \omega_i D_{ij} \mathbf{f}_{(j,i)}^{\text{vol}} = 0, \quad (104)$$

where J is the element Jacobian, ω_i are the quadrature weights, $D_{ij} = l'_j(\xi_i)$ is the differentiation matrix derived from the Lagrange basis and $\mathbf{f}_{(i,j)}^*$ is the numerical two-point surface flux, and $\mathbf{f}_{(j,i)}^{\text{vol}}$ is the volume numerical two-point symmetric flux. Moreover, the differentiation matrix satisfies the summation-by-parts (SBP) property

$$(MD) + (MD)^T = \mathbf{Q} + \mathbf{Q}^T = \mathbf{B}, \quad (105)$$

where M is the diagonal mass matrix and $Q_{ij} = \omega_i D_{ij}$ [22].

A natural extension of the non-conservative products in the FV method is the DGSEM discretization (see, e.g., [17, 21])

$$J\dot{\mathbf{u}}_i = - \sum_{j=0}^N 2Q_{ij} \mathbf{f}_{(i,j)}^{\text{vol}} - \delta_{iN} \mathbf{f}_N + \delta_{i0} \mathbf{f}_0 + \sum_{j=0}^N Q_{ij} \mathbf{g}_{(i,j)}^{\text{vol}} - \mathbf{f}_{(N,R)}^* \delta_{iN} - \mathbf{f}_{(0,L)}^* \delta_{i0} + \mathbf{g}_{(N,R)}^* \frac{\delta_{iN}}{2} - \mathbf{g}_{(0,L)}^* \frac{\delta_{i0}}{2}, \quad (106)$$

where $\mathbf{g}_{(i,j)}^*$ is the surface numerical non-conservative flux and \mathbf{g}^{vol} is the volume numerical non-conservative flux. Rueda-Ramirez et al. [50] showed that the DGSEM semi-discretization (106) can be rewritten as flux differencing formula, if the non-conservative terms can be written as the product of a local and a symmetric contribution, i.e.,

$$\mathbf{g}_{(j,k)}^{\text{vol}} = \mathbf{g}_{(j,k)}^{\text{sym}} \circ \mathbf{g}_j. \quad (107)$$

Here, we extend this result to non-conservative terms that are anti-symmetric, i.e., terms that can be written as the product of a symmetric contribution and an anti-symmetric contribution.

Lemma 5.1. *It is possible to rewrite (106) as a flux-difference formula,*

$$J\omega_j \dot{\mathbf{u}}_j = \mathbf{\Gamma}_{(j,j-1)} - \mathbf{\Gamma}_{(j,j+1)} \quad j = 0, \dots, N, \quad (108)$$

where the indexes $j = -1$ and $j = N$ refer to the outer states (across the left and right boundaries, respectively) and $\mathbf{\Gamma}_{j,k}$ is the so-called staggered (or telescoping) “flux” between node j and the adjacent node k , if it is possible to write the volume numerical non-conservative term as a product of an anti-symmetric and a symmetric contribution, i.e.,

$$\mathbf{g}_{(j,k)}^{\text{vol}} = \mathbf{g}_{(j,k)}^{\text{sym}} \circ \llbracket \mathbf{g} \rrbracket_{(j,k)}. \quad (109)$$

Proof. The anti-symmetric (jump) term can be rewritten as

$$\llbracket \mathbf{g} \rrbracket_{(j,k)} = 2 \{ \{ \mathbf{g} \} \}_{(j,k)} - 2\mathbf{g}_j. \quad (110)$$

Thus, the volume term reads

$$\mathbf{g}_{(j,k)}^{\text{vol}} = 2\mathbf{g}_{(j,k)}^{\text{sym}} \circ \{ \{ \mathbf{g} \} \}_{(j,k)} - 2\mathbf{g}_{(j,k)}^{\text{sym}} \circ \mathbf{g}_j, \quad (111)$$

where the first term is purely symmetric, and the second term is the product of a symmetric and a local contribution. Therefore, the rest of proof follows the same steps as the flux differencing lemma in [50]. \square

The anti-symmetric flux (109) is zero when evaluated on a single point: $\mathbf{g}^*(\mathbf{u}_j, \mathbf{u}_j) = 0$. Given the anti-symmetric property of the non-conservative flux, we can rewrite our discretization as

$$J\omega_i \dot{\mathbf{u}}_i = - \left(\sum_{j=0}^N \omega_i 2D_{ij} \mathbf{f}_{(i,j)}^{\text{vol}} - \delta_{iN} \mathbf{f}_N + \delta_{i0} \mathbf{f}_0 + \sum_{j=0}^N \omega_i D_{ij} \mathbf{g}_{(i,j)}^{\text{vol}} \right) - \left(\mathbf{f}_{(N,R)}^* \delta_{iN} - \mathbf{f}_{(0,L)}^* \delta_{i0} + \mathbf{g}_{(N,R)}^* \frac{\delta_{iN}}{2} - \mathbf{g}_{(0,L)}^* \frac{\delta_{i0}}{2} \right). \quad (112)$$

Note that the non-conservative anti-symmetric flux also reduces computational cost in the volume term, as it avoids the diagonal contributions and requires computing only the off-diagonal terms, either from the upper or the lower triangle of the matrix, similar to the contribution of the conservative symmetric volume flux [48].

5.1 Conservation properties of DGSEM

In this section we extend the FV properties of the numerical fluxes for the non-conservative product of the geopotential term to the DGSEM. First, we extend the result of Lemma 4.1.

Lemma 5.2. *Given the set of variables $(\varrho, \varrho v, \varrho\theta)$, a numerical non-conservative surface and volume flux $g_{\varrho v}$ and the corresponding DGSEM discretization (106) are TEC if*

(i) *the density and non conservative fluxes are of the form*

$$f^{\varrho,*} = f^{\varrho,\text{vol}} = \bar{\varrho} \{v\}, \quad g^{\varrho v,*} = g^{\varrho v,\text{vol}} = \bar{\varrho} \llbracket \phi \rrbracket, \quad (113)$$

(ii) *and the numerical flux $(f_{\varrho}, f_{\varrho v}, f_{\varrho\theta})$ is of the form (28) or (30).*

Proof. Since the proof mimics the steps for the FV framework, we only present the main steps. We introduce the generic anti-symmetric volume and surface numerical flux

$$g^{\varrho v,*} = g^{\varrho v,\text{vol}} = \bar{\varrho} \llbracket \phi \rrbracket, \quad (114)$$

and we define the entropy variables

$$\mathbf{q} = \begin{pmatrix} -\frac{1}{2} \frac{m^2}{\varrho^2} + \phi \\ \frac{m}{\varrho} \\ \frac{\gamma}{\gamma-1} K \left(\frac{\varrho}{\varrho\theta} \right)^{\gamma-1} \end{pmatrix} = \begin{pmatrix} -\frac{1}{2} \frac{m^2}{\varrho^2} \\ \frac{m}{\varrho} \\ \frac{\gamma}{\gamma-1} K \left(\frac{\varrho}{\varrho\theta} \right)^{\gamma-1} \end{pmatrix} + \begin{pmatrix} \phi \\ 0 \\ 0 \end{pmatrix} = \mathbf{v} + \phi \mathbf{e}_1. \quad (115)$$

Since the conservative numerical flux is TEC,

$$\llbracket \mathbf{v}^T \rrbracket \mathbf{f}^{\text{num}} = \llbracket \psi \rrbracket. \quad (116)$$

We can contract in entropy space

$$\sum_{i=0}^N \mathbf{v}_i^T \mathbf{M} J \dot{\mathbf{u}}_i = \langle \mathbf{v}, J \dot{\mathbf{u}} \rangle_{\mathbf{M}} = J \dot{\eta}. \quad (117)$$

In the following proof we drop the term \mathbf{M} , and divide the volume contribution VOL and the surface contribution SURF:

$$\begin{aligned} J \dot{\eta} &= - \sum_{i=0}^N \mathbf{v}_i^T \left(\sum_{j=0}^N 2 \mathbf{Q}_{ij} \mathbf{f}_{(i,j)}^{\text{vol}} - \delta_{iN} \mathbf{f}_N + \delta_{i0} \mathbf{f}_0 + \sum_{j=0}^N \mathbf{Q}_{ij} \mathbf{g}_{(i,j)}^{\text{vol}} \right) \\ &\quad - \sum_{i=0}^N \mathbf{v}_i^T \left(\mathbf{f}_{(N,R)}^* \delta_{iN} - \mathbf{f}_{(0,L)}^* \delta_{i0} + \mathbf{g}_{(N,R)}^* \frac{\delta_{iN}}{2} - \mathbf{g}_{(0,L)}^* \frac{\delta_{i0}}{2} \right) \\ &= - \text{VOL} - \text{SURF}. \end{aligned} \quad (118)$$

We first consider the volume term:

$$\begin{aligned} \text{VOL} &= \sum_{i=0}^N \mathbf{q}_i^T \left(\sum_{j=0}^N 2 \mathbf{Q}_{ij} \mathbf{f}_{(i,j)}^{\text{vol}} - \delta_{iN} \mathbf{f}_N + \delta_{i0} \mathbf{f}_0 + \sum_{j=0}^N \mathbf{Q}_{ij} \mathbf{g}_{(i,j)}^{\text{vol}} \right) \\ &= \sum_{i,j=0}^N \mathbf{q}_i^T \mathbf{Q}_{ij} \mathbf{f}_{(i,j)}^{\text{vol}} - \mathbf{q}_N^T \mathbf{f}_N + \mathbf{q}_0^T \mathbf{f}_0 + \sum_{i,j=0}^N \mathbf{q}_i^T \mathbf{Q}_{ij} \mathbf{g}_{(i,j)}^{\text{vol}}. \end{aligned} \quad (119)$$

By applying the SBP property $\mathbf{Q}_{ij} = \mathbf{B}_{ij} - \mathbf{Q}_{ji} + \mathbf{Q}_{ij}$,

$$\text{VOL} = \sum_{i,j=0}^N \mathbf{q}_i^T (\mathbf{B}_{ij} - \mathbf{Q}_{ji} + \mathbf{Q}_{ij}) \mathbf{f}_{(i,j)}^{\text{vol}} - \mathbf{q}_N^T \mathbf{f}_N + \mathbf{q}_0^T \mathbf{f}_0 + \frac{1}{2} \sum_{i,j=0}^N \mathbf{q}_i^T (\mathbf{B}_{ij} - \mathbf{Q}_{ji} + \mathbf{Q}_{ij}) \mathbf{g}_{(i,j)}^{\text{vol}}. \quad (120)$$

Because of the flux consistency on the diagonal elements and the definition of \mathbf{B} , we have

$$\text{VOL} = \sum_{i,j=0}^N \mathbf{q}_i^T (-\mathbf{Q}_{ji} + \mathbf{Q}_{ij}) \mathbf{f}_{(i,j)}^{\text{vol}} + \frac{1}{2} \sum_{i,j=0}^N \mathbf{q}_i^T (-\mathbf{Q}_{ji} + \mathbf{Q}_{ij}) \mathbf{g}_{(i,j)}^{\text{vol}}. \quad (121)$$

Since the $f_{(i,j)} = f_{(j,i)}$ is symmetric and $g_{(i,j)} = -g_{(j,i)}$ is anti-symmetric, we can rearrange and reindex

$$\text{VOL} = \sum_{i,j=0}^N (\mathbf{q}_i^T - \mathbf{q}_j^T) \mathbf{Q}_{ij} \mathbf{f}_{(i,j)}^{\text{vol}} + \frac{1}{2} \sum_{i,j=0}^N (\mathbf{q}_i^T + \mathbf{q}_j^T) \mathbf{Q}_{ij} \mathbf{g}_{(i,j)}^{\text{vol}}. \quad (122)$$

Applying the definition of TEC flux, we are left with

$$\text{VOL} = \sum_{i,j=0}^N \mathbf{Q}_{ij} (\psi_i - \psi_j) + \sum_{i,j=0}^N (\phi_i - \phi_j) \mathbf{Q}_{ij} \mathbf{f}_{(i,j)}^e + \frac{1}{2} \sum_{i,j=0}^N (v_i + v_j) \mathbf{Q}_{ij} \bar{\varrho}_{i,j} (\phi_j - \phi_i). \quad (123)$$

Because of the form of the density flux and by applying the properties of the differential operator \mathbf{Q} we have $\text{VOL} = \psi_0 - \psi_N$. Now that we simplified the volume term, we can sum also the surface term

$$J\dot{\eta} = -\text{VOL} - \text{SURF} = \psi_N - \psi_0 - \mathbf{q}_N^T \mathbf{f}_{(N,R)}^* + \mathbf{q}_0^T \mathbf{f}_{(0,L)}^* - \mathbf{q}_N^T \frac{u_N}{2} \mathbf{g}_{(N,R)}^* + \mathbf{q}_0^T \frac{u_0}{2} \mathbf{g}_{(0,L)}^*. \quad (124)$$

The proof now proceeds as for the FV method. \square

The remaining properties are straightforward following the same steps as in the above lemma.

5.2 Well-balanced DGSEM

Lemma 5.3. *The DGSEM discretization (106) with non-conservative surface and volume fluxes $g_{(i,j)}^*$, $g_{(i,j)}^{\text{vol}}$ preserves the hydrostatic balance prescribed by a constant background temperature T of the compressible Euler equations if*

(i) *the numerical non-conservative fluxes are of the form*

$$g^* = g^{\text{vol}} = \{\{\varrho\}\}_{\log} \llbracket \phi \rrbracket, \quad (125)$$

(ii) *and the pressure term is discretized as $\{\{p\}\}$.*

Proof. The semi-discretization (106) applied to the Euler equations and considering a background state reduces for $i = 1$ to

$$\begin{aligned} -\{\{p\}\} + p_R - \{\{\varrho\}\}_{\log} \frac{\phi_L - \phi_R}{2} + 2 \sum_{j=0}^N \omega_i D_{ij} \left(\{\{p^k\}\}_{i,j} + \bar{\varrho}_{i,j} \frac{\llbracket \phi \rrbracket_{j,i}}{2} \right) \\ = -\{\{p\}\} + p_R + \{\{\varrho\}\}_{\log} \frac{\llbracket \phi \rrbracket}{2} + 2 \sum_{j=0}^N \omega_i D_{ij} \left(\{\{p\}\}_{i,j} + \bar{\varrho}_{i,j} \frac{\llbracket \phi \rrbracket_{j,i}}{2} \right). \end{aligned} \quad (126)$$

Substituting the solution for the isothermal background balance $\llbracket \log(\varrho) \rrbracket = -\llbracket \phi \rrbracket / (RT)$ yields

$$-RT \{\{\varrho\}\} + RT \varrho_R + RT \frac{\llbracket \varrho \rrbracket}{2} + 2 \sum_{j=0}^N \omega_i D_{ij} \left(\frac{p_j}{2} - RT \frac{\llbracket \varrho \rrbracket}{2} \right) = 2 \sum_{j=0}^N \omega_i D_{ij} \left(\frac{p_j}{2} + RT \frac{\varrho_j}{2} \right) = 0. \quad (127)$$

For the case $i = N$ and general i , the proof follows the same steps. \square

Lemma 5.4. *The DGSEM discretization (106) non-conservative surface and volume flux $g_{(i,j)}^*$, $g_{(i,j)}^{\text{vol}}$ preserves the hydrostatic balance prescribed by a constant background potential temperature θ of the compressible Euler equations if*

(i) *the numerical non-conservative fluxes are of the form*

$$g_{(i,j)}^* = g_{(i,j)}^{\text{vol}} = \{\{\varrho\}\}_{\gamma} \llbracket \phi \rrbracket, \quad (128)$$

(ii) *and the pressure term is discretized as $\{\{p\}\}$.*

Proof. The proof follows the same steps as the one of Lemma 5.3. \square

6 Extension to three-dimensional curvilinear meshes

In this work, we recall the main ingredients of the DGSEM curvilinear formulation, following closely the notation introduced in [51], see also [17, 21]. On a three-dimensional curvilinear element, the semi-discrete DGSEM formulation for the advective and non-conservative contributions can be written in compact form as

$$J_{ijk} \omega_{ijk} \dot{\mathbf{u}}_{ijk} = \mathcal{F}_{ijk}, \quad (129)$$

where J_{ijk} denotes the mapping Jacobian, ω_{ijk} the quadrature weight at node (i, j, k) , and \mathcal{F}_{ijk} the discrete operator collecting all numerical flux contributions in the three spatial directions.

An explicit expression of the operator reads

$$\begin{aligned} \mathcal{F}_{ijk} = & \omega_{jk} \left(-2 \sum_{m=0}^N Q_{im} \tilde{\mathbf{f}}_{(i,m)jk}^{1,\text{vol}} - \sum_{m=0}^N Q_{im} \tilde{\mathbf{g}}_{(i,m)jk}^1 - \delta_{i0} \left[\left(\tilde{\mathbf{f}} + \frac{\tilde{\mathbf{g}}}{2} \right) \cdot J\mathbf{a}^1 \right]_{0jk} + \delta_{iN} \left[\left(\tilde{\mathbf{f}} + \frac{\tilde{\mathbf{g}}}{2} \right) \cdot J\mathbf{a}^1 \right]_{Njk} \right. \\ & - 2 \sum_{m=0}^N Q_{jm} \tilde{\mathbf{f}}_{i(j,m)k}^{2,\text{vol}} - \sum_{m=0}^N Q_{jm} \tilde{\mathbf{g}}_{i(j,m)k}^2 - \delta_{j0} \left[\left(\tilde{\mathbf{f}} + \frac{\tilde{\mathbf{g}}}{2} \right) \cdot J\mathbf{a}^2 \right]_{i0k} + \delta_{jN} \left[\left(\tilde{\mathbf{f}} + \frac{\tilde{\mathbf{g}}}{2} \right) \cdot J\mathbf{a}^2 \right]_{iNk} \\ & \left. - 2 \sum_{m=0}^N Q_{km} \tilde{\mathbf{f}}_{ij(k,m)}^{3,\text{vol}} - \sum_{m=0}^N Q_{km} \tilde{\mathbf{g}}_{ij(k,m)}^3 - \delta_{k0} \left[\left(\tilde{\mathbf{f}} + \frac{\tilde{\mathbf{g}}}{2} \right) \cdot J\mathbf{a}^3 \right]_{ij0} + \delta_{kN} \left[\left(\tilde{\mathbf{f}} + \frac{\tilde{\mathbf{g}}}{2} \right) \cdot J\mathbf{a}^3 \right]_{ijN} \right) \\ & + \omega_{jk} \left(\delta_{i0} \left[\tilde{\mathbf{f}}_{(0,L)jk}^* + \frac{1}{2} \tilde{\mathbf{g}}_{(0,L)jk}^* \right] - \delta_{iN} \left[\tilde{\mathbf{f}}_{(N,R)jk}^* + \frac{1}{2} \tilde{\mathbf{g}}_{(N,R)jk}^* \right] \right) \\ & + \omega_{ik} \left(\delta_{j0} \left[\tilde{\mathbf{f}}_{i(0,L)k}^* + \frac{1}{2} \tilde{\mathbf{g}}_{i(0,L)k}^* \right] - \delta_{jN} \left[\tilde{\mathbf{f}}_{i(N,R)k}^* + \frac{1}{2} \tilde{\mathbf{g}}_{i(N,R)k}^* \right] \right) \\ & + \omega_{ij} \left(\delta_{k0} \left[\tilde{\mathbf{f}}_{ij(0,L)}^* + \frac{1}{2} \tilde{\mathbf{g}}_{ij(0,L)}^* \right] - \delta_{kN} \left[\tilde{\mathbf{f}}_{ij(N,R)}^* + \frac{1}{2} \tilde{\mathbf{g}}_{ij(N,R)}^* \right] \right). \end{aligned} \quad (130)$$

Here, $Q_{ij} = \omega_i D_{ij}$ is the SBP matrix, and \mathbf{a}_{ijk}^m are the contravariant basis vectors linking the reference coordinates $(\xi^1, \xi^2, \xi^3) \in [-1, 1]^3$ to the physical domain. The symbol $\tilde{\mathbf{g}}$ accounts for additional non-conservative terms. The numerical two-point fluxes in the three directions are consistently defined with the metric terms, e.g.,

$$\tilde{\mathbf{f}}_{(i,m)jk}^{1,\text{vol}} = \overset{\leftrightarrow}{\mathbf{f}}^{\text{vol}}(\mathbf{u}_{ijk}, \mathbf{u}_{mjk}) \cdot \{ \{ J\mathbf{a}^1 \} \}_{(i,m)jk}, \quad (131)$$

$$\tilde{\mathbf{f}}_{i(j,m)k}^{2,\text{vol}} = \overset{\leftrightarrow}{\mathbf{f}}^{\text{vol}}(\mathbf{u}_{ijk}, \mathbf{u}_{imk}) \cdot \{ \{ J\mathbf{a}^2 \} \}_{i(j,m)k}, \quad (132)$$

$$\tilde{\mathbf{f}}_{ij(k,m)}^{3,\text{vol}} = \overset{\leftrightarrow}{\mathbf{f}}^{\text{vol}}(\mathbf{u}_{ijk}, \mathbf{u}_{ijm}) \cdot \{ \{ J\mathbf{a}^3 \} \}_{ij(k,m)}, \quad (133)$$

where we adopted the common notation $\overset{\leftrightarrow}{\mathbf{f}}$ to denote block vectors, containing a state vector in each spatial component (see, e.g., [7, 66])

$$\overset{\leftrightarrow}{\mathbf{f}} = \begin{bmatrix} \mathbf{f}_1 \\ \mathbf{f}_2 \\ \mathbf{f}_3 \end{bmatrix}, \quad \overset{\leftrightarrow}{\mathbf{g}} = \begin{bmatrix} \mathbf{g}_1 \\ \mathbf{g}_2 \\ \mathbf{g}_3 \end{bmatrix}, \quad (134)$$

with each component defined as follows

$$\mathbf{f}_1 = \begin{pmatrix} \varrho u \\ \varrho u^2 + p \\ \varrho uv \\ \varrho uw \\ \varrho \theta u \end{pmatrix}, \quad \mathbf{f}_2 = \begin{pmatrix} \varrho v \\ \varrho v^2 + p \\ \varrho vw \\ \varrho \theta v \end{pmatrix}, \quad \mathbf{f}_3 = \begin{pmatrix} \varrho w \\ \varrho wu \\ \varrho wv \\ \varrho w^2 + p \\ \varrho \theta w \end{pmatrix}, \quad \mathbf{g}_i = \varrho \phi \begin{pmatrix} 0 \\ \delta_{i1} \\ \delta_{i2} \\ \delta_{i3} \\ 0 \end{pmatrix} = \mathbf{g}_i = \varrho \phi, \quad i = 1, 2, 3. \quad (135)$$

The non-conservative and anti-symmetric volume fluxes are defined as

$$\tilde{\mathbf{g}}_{(i,m)jk}^{1,\text{vol}} = \overset{\leftrightarrow}{\mathbf{g}}^{\text{vol}}(\mathbf{u}_{ijk}, \mathbf{u}_{mjk}) \cdot \{ \{ J\mathbf{a}^1 \} \}_{(i,m)jk}, \quad (136)$$

$$\tilde{\mathbf{g}}_{i(j,m)k}^{2,\text{vol}} = \overset{\leftrightarrow}{\mathbf{g}}^{\text{vol}}(\mathbf{u}_{ijk}, \mathbf{u}_{imk}) \cdot \{ \{ J\mathbf{a}^2 \} \}_{i(j,m)k}, \quad (137)$$

$$\tilde{\mathbf{g}}_{ij(k,m)}^{3,\text{vol}} = \overset{\leftrightarrow}{\mathbf{g}}^{\text{vol}}(\mathbf{u}_{ijk}, \mathbf{u}_{ijm}) \cdot \{ \{ J\mathbf{a}^3 \} \}_{ij(k,m)}. \quad (138)$$

The surface numerical flux is defined similarly as

$$\tilde{\mathbf{f}}_{(i,m)jk}^{1,*} = \overset{\leftrightarrow}{\mathbf{f}}^* (\mathbf{u}_{ijk}, \mathbf{u}_{mjk}) \cdot \{\{J\mathbf{a}^1\}\}_{(i,m)jk}, \quad (139)$$

$$\tilde{\mathbf{f}}_{(j,m)k}^{2,*} = \overset{\leftrightarrow}{\mathbf{f}}^* (\mathbf{u}_{ijk}, \mathbf{u}_{imk}) \cdot \{\{J\mathbf{a}^2\}\}_{(j,m)k}, \quad (140)$$

$$\tilde{\mathbf{f}}_{ij(k,m)}^{3,*} = \overset{\leftrightarrow}{\mathbf{f}}^* (\mathbf{u}_{ijk}, \mathbf{u}_{ijm}) \cdot \{\{J\mathbf{a}^3\}\}_{ij(k,m)}. \quad (141)$$

6.1 TEC and KPEP with curvilinear coordinates

In this section, we consider the compressible Euler equations with the potential temperature and extend the property for TEC. The extension of the other results presented in the previous 1D Cartesian semi-discretization is straightforward, following the same approach, therefore we will only state them.

Theorem 6.1. *Given a semi-discretization of the compressible Euler equations as in (130), for the set of conserved variables $(\varrho, \varrho\mathbf{V}, \varrho\theta)$, a numerical non-conservative surface and volume fluxes, a numerical conservative surface and volume fluxes are TEC if*

(i) *the numerical density flux and non-conservative fluxes are of the form*

$$\mathbf{f}^{\varrho,*} = \mathbf{f}^{\varrho,\text{vol}} = \bar{\varrho} \{\{\mathbf{V}\}\}, \quad \mathbf{g}^{\varrho\mathbf{V},*} = \mathbf{g}^{\varrho\mathbf{V},\text{vol}} = \bar{\varrho} \{\{\phi\}\}, \quad (142)$$

(ii) *and the numerical flux $(f_\varrho, f_{\varrho\mathbf{V}}, f_{\varrho\theta})$ is of the form (28).*

Proof. Consider the first volume term in the ξ_1 direction and contract it in the entropy variable space, where the entropy variables are here denoted with \mathbf{v} , to avoid confusion with the weights ω_{ijk} .

$$\sum_{i=0}^N \mathbf{v}_{ijk}^T \mathbf{VOL}^1 = \omega_{jk} \sum_{i=0}^N \mathbf{v}_{ijk}^T \left(-2 \sum_{m=0}^N Q_{im} \tilde{\mathbf{f}}_{(i,m)jk}^{1,\text{vol}} - \sum_{m=0}^N Q_{im} \tilde{\mathbf{g}}_{(i,m)jk}^1 - \delta_{i0} \left[\overset{\leftrightarrow}{\mathbf{f}} \cdot J\mathbf{a}^1 \right]_{0jk} + \delta_{iN} \left[\overset{\leftrightarrow}{\mathbf{f}} \cdot J\mathbf{a}^1 \right]_{Njk} \right). \quad (143)$$

Applying the SBP property $\mathbf{Q}_{ij} = B_{ij} - Q_{ji} + Q_{ij}$, we can write

$$\begin{aligned} \sum_{i=0}^N \mathbf{v}_{ijk}^T \mathbf{VOL}^1 = & \omega_{jk} \sum_{i=0}^N \mathbf{v}_{ijk}^T \left(-2 \sum_{m=0}^N (B_{ij} - Q_{ji} + Q_{ij}) \tilde{\mathbf{f}}_{(i,m)jk}^{1,\text{vol}} - \sum_{m=0}^N (B_{ij} - Q_{ji} + Q_{ij}) \tilde{\mathbf{g}}_{(i,m)jk}^1 \right. \\ & \left. - \delta_{i0} \left[\overset{\leftrightarrow}{\mathbf{f}} \cdot J\mathbf{a}^1 \right]_{0jk} + \delta_{iN} \left[\overset{\leftrightarrow}{\mathbf{f}} \cdot J\mathbf{a}^1 \right]_{Njk} \right). \end{aligned} \quad (144)$$

Because of the flux consistency on the diagonal elements and the definition of \mathbf{B} , we have

$$\sum_{i=0}^N \mathbf{v}_{ijk}^T \mathbf{VOL}^1 = \omega_{jk} \left(- \sum_{i,m=0}^N \mathbf{v}_{ijk}^T (-Q_{ji} + Q_{ij}) \tilde{\mathbf{f}}_{(i,m)jk}^{1,\text{vol}} - \frac{1}{2} \sum_{i,m=0}^N \mathbf{v}_{ijk}^T (-Q_{ji} + Q_{ij}) \tilde{\mathbf{g}}_{(i,m)jk}^1 \right). \quad (145)$$

Here the proof closely follows the step for the 1D DGSEM; indeed, due to the symmetry and anti-symmetric properties of the conservative and non-conservative fluxes, after a rearrangement of the index, we are left with

$$\sum_{i=0}^N \mathbf{v}_{ijk}^T \mathbf{VOL}^1 = \omega_{jk} \left(- \sum_{i,m=0}^N Q_{im} (\mathbf{v}_{ijk}^T - \mathbf{v}_{mjk}^T) \tilde{\mathbf{f}}_{(i,m)jk}^{1,\text{vol}} - \frac{1}{2} \sum_{i,m=0}^N Q_{im} (\mathbf{v}_{ijk}^T + \mathbf{v}_{mjk}^T) \tilde{\mathbf{g}}_{(i,m)jk}^1 \right). \quad (146)$$

Applying the definition of TEC flux and the non-conservative flux, we can write

$$\sum_{i=0}^N \mathbf{v}_{ijk}^T \mathbf{VOL}^1 = \omega_{jk} \left(- \sum_{i,m=0}^N Q_{im} \{\{J\mathbf{a}\}\}_{(i,m)jk} \cdot (\psi_{ijk} - \psi_{mjk}) \right). \quad (147)$$

The difference now with the 1D Cartesian case is the presence of the metric terms. After some manipulations and re-indexing, the term simplifies to

$$\sum_{i=0}^N \mathbf{v}_{ijk}^T \mathbf{VOL}^1 = \omega_{jk} \left(- \sum_{i,m=0}^N Q_{im} (J\mathbf{a}^1)_{mjk} \cdot \psi_{ijk} + (J\mathbf{a}^1)_{0jk} \cdot \psi_{0jk} - (J\mathbf{a}^1)_{Njk} \cdot \psi_{Njk} \right). \quad (148)$$

The remaining terms can be treated similarly, as well as the surface term, that we do not report here for brevity. We are left with

$$- \sum_{i,j,k=0}^N \omega_{ijk} \psi_{ijk} \cdot \sum_{m=0}^N \left(D_{im} (J\mathbf{a}^1)_{mj k} + D_{jm} (J\mathbf{a}^2)_{im k} + D_{km} (J\mathbf{a}^3)_{ij m} \right) = 0, \quad (149)$$

which is equal to zero if the discrete metric identity [33] is satisfied. \square

Theorem 6.2. *Given a semi-discretization of the compressible Euler equations as in (130), for the set of conserved variables $(\varrho, \varrho\mathbf{V}, \varrho E)$, a numerical non-conservative surface and volume fluxes, a numerical conservative surface and volume fluxes are TEC if the numerical density flux and the non-conservative fluxes are of the form*

$$\mathbf{f}^{\varrho,*} = \mathbf{f}^{\varrho,\text{vol}} = \bar{\varrho} \{\{\mathbf{V}\}\}, \quad \mathbf{g}^{\varrho\mathbf{V},*} = \mathbf{g}^{\varrho\mathbf{V},\text{vol}} = \bar{\varrho} \llbracket \phi \rrbracket, \quad \mathbf{g}^{\varrho E,*} = \mathbf{g}^{\varrho E,\text{vol}} = \mathbf{f}^{\varrho} \llbracket \phi \rrbracket. \quad (150)$$

Theorem 6.3. *Given a semi-discretization of the compressible Euler equations as in (130), for the set of conserved variables $(\varrho, \varrho\mathbf{V}, \varrho E)$ or $(\varrho, \varrho\mathbf{V}, \varrho\theta)$, a numerical non-conservative surface and volume fluxes, a numerical conservative surface and volume fluxes are KPEP if*

(i) *the numerical density flux and the non-conservative fluxes are of the form*

$$\mathbf{f}^{\varrho,*} = \mathbf{f}^{\varrho,\text{vol}} = \bar{\varrho} \{\{\mathbf{V}\}\}, \quad \mathbf{g}^{\varrho\mathbf{V},*} = \mathbf{g}^{\varrho\mathbf{V},\text{vol}} = \bar{\varrho} \llbracket \phi \rrbracket, \quad (151)$$

(ii) *and the numerical flux is KEP.*

6.2 Well-balancedness with curvilinear coordinates

Theorem 6.4. *Given a semi-discretization of the compressible Euler equations as in (130), for the set of conserved variables $(\varrho, \varrho\mathbf{V}, X)$, where X represents any conserved variable that closes the system, a non-conservative numerical surface and volume flux \mathbf{g} preserve the hydrostatic balance prescribed by a constant background temperature T under any coordinate mapping if*

(i) *the non-conservative volume flux is of the form*

$$\mathbf{g}^{\varrho\mathbf{V},\text{vol}} = \{\{\varrho\}\}_{\log} \llbracket \phi \rrbracket, \quad (152)$$

(ii) *the pressure term is discretized as $\{\{p\}\}$,*

(iii) *and the free-stream preservation property is satisfied at the discrete level.*

Proof. For sake of simplicity and brevity, here we present the proof for 2D case only in the x momentum.

We start by observing that the surface non-conservative fluxes are zeros, because of the continuity of the potential along the interfaces, i.e.,

$$\phi_{0j}^R = \phi_{Nj}, \quad \phi_{0j} = \phi_{Nj}^L, \quad \phi_{i0}^R = \phi_{iN}, \quad \phi_{i0} = \phi_{iN}^L. \quad (153)$$

Therefore, the semidiscrete formulation can be rewritten at the hydrostatic balance for the horizontal momentum equation as

$$\begin{aligned} & J_{ij}(\varrho u)_{ij} + \frac{1}{\omega_i} \left(Ja_{1,Nj}^1 \left(\{\{p\}\}_{(N,R)j} - p_{Nj} \right) \delta_{iN} - Ja_{1,0j}^1 \left(\{\{p\}\}_{(0,L)} - p_{0j} \right) \delta_{i0} \right) \\ & + \frac{1}{\omega_j} \left(Ja_{1,iN}^2 \left(\{\{p\}\}_{i,(N,R)} - p_{iN} \right) \delta_{jN} - Ja_{1,i0}^2 \left(\{\{p\}\}_{i,(0,L)} - p_{i0} \right) \delta_{j0} \right) \\ & + \sum_{k=0}^N 2D_{ik} \{\{Ja_1^1\}\}_{(i,k)j} \left(\{\{p\}\}_{(i,k)j} + \frac{1}{2} \{\{\varrho\}\}_{\log,(i,k)j} (\phi_{kj} - \phi_{ij}) \right) \\ & + \sum_{k=0}^N 2D_{jk} \{\{Ja_1^2\}\}_{i(j,k)} \left(\{\{p\}\}_{(i(j,k))} + \frac{1}{2} \{\{\varrho\}\}_{\log,i(j,k)} (\phi_{ik} - \phi_{ij}) \right) = 0. \end{aligned} \quad (154)$$

The analytical solution of an isothermal hydrostatic flow are

$$p = p_0 e^{-\phi/RT} \quad \varrho = \frac{p_0}{RT} e^{-\phi/RT}. \quad (155)$$

Considering the first surface conservative term, we have

$$\frac{p_{Nj}}{2} - \frac{p_{0j}^R}{2} = \frac{p_0}{2} \left(e^{-\phi_{Nj}/RT} - e^{-\phi_{0j}^R/RT} \right) = 0, \quad (156)$$

which is again zero for the continuity of the potential along the interfaces. The same applies to all the remaining surface terms.

For the volume terms we just consider the first one

$$\text{VOL}^1 = \sum_{k=0}^N 2D_{ik} \{ \{ Ja_1^1 \} \}_{(i,k)j} \left(\frac{p_{kj} + p_{ij}}{2} + \frac{1}{2} \frac{\varrho_{kj} - \varrho_{ij}}{\log(\varrho_{kj}) - \log(\varrho_{ij})} (\phi_{kj} - \phi_{ij}) \right). \quad (157)$$

From the hydrostatic balance, we derive $\llbracket \log(\varrho) \rrbracket = -\frac{\llbracket \phi \rrbracket}{RT}$ thus

$$\text{VOL}^1 = \sum_{k=0}^N 2D_{ik} \{ \{ Ja_1^1 \} \}_{(i,k)j} \left(RT \frac{\varrho_{kj} + \varrho_{ij}}{2} - RT \frac{1}{2} (\varrho_{kj} - \varrho_{ij}) \right) = \sum_{k=0}^N 2D_{ik} \{ \{ Ja_1^1 \} \}_{(i,k)j} RT \varrho_{ij}. \quad (158)$$

The second volume term is analogous

$$\begin{aligned} \text{VOL}^2 &= \sum_{k=0}^N 2D_{jk} \{ \{ Ja_1^2 \} \}_{i(j,k)} \left(\frac{p_{ik} + p_{ij}}{2} + \frac{1}{2} \frac{\varrho_{ik} - \varrho_{ij}}{\log(\varrho_{ik}) - \log(\varrho_{ij})} (\phi_{ik} - \phi_{ij}) \right) \\ &= \sum_{k=0}^N 2D_{jk} \{ \{ Ja_1^2 \} \}_{i(j,k)} RT \varrho_{ij}. \end{aligned} \quad (159)$$

Summing up all the volume terms

$$\text{VOL} = \text{VOL}^1 + \text{VOL}^2 = 2RT \varrho_{ij} \sum_{k=0}^N \left(D_{ik} \{ \{ Ja_1^1 \} \}_{(i,k),j} + D_{jk} \{ \{ Ja_1^2 \} \}_{i(j,k)} \right) = 0, \quad (160)$$

which is equal to zero, due to the free-stream preservation property. \square

Theorem 6.5. *Given a semi-discretization of the compressible Euler equations as in (130), for the set of conserved variables $(\varrho, \varrho \mathbf{V}, X)$, where X represents any conserved variable that closes the system, a non-conservative numerical volume and surface flux \mathbf{g} preserve the hydrostatic balance prescribed by a constant background potential temperature θ under any coordinate mapping if*

(i) *the non-conservative volume flux is of the form*

$$\mathbf{g}^{\varrho \mathbf{V}, \text{vol}} = \{ \{ \varrho \} \}_\gamma \llbracket \phi \rrbracket, \quad (161)$$

(ii) *the pressure term is discretized as $\{ \{ p \} \}$,*

(iii) *and the free-stream preservation property is satisfied at the discrete level.*

Proof. The proof is conceptually analogous to the previous theorem. \square

7 Numerical results

Next, we present numerical results for both set of equations (1), (2), assessing the theoretical findings described in the previous sections. We have implemented our novel methods in Julia [5] using Trixi.jl [49, 52]. The time integration method is SSPRK43 [35] implemented in OrdinaryDiffEq.jl [42] and, unless stated otherwise, the fixed Courant number is taken to be 1. The conservative surface flux, except for the test cases to assess the conservation of entropy and total energy, is computed with the low Mach number approximate Riemann solver (LMARS) numerical flux [13]. We used Makie.jl [14] and matplotlib [28] for visualization. All source code required to reproduce the numerical results presented here is available online in our reproducibility repository [1].

The results are presented as follows: first, we assess the conservation of entropy and total energy for the potential temperature formulation. We then show numerical results for well-balanced schemes on curvilinear meshes, followed by a convergence analysis on Cartesian and curvilinear meshes for the inertia–gravity waves test case. A comparison between the total energy and potential temperature formulations is then carried out on mountain-wave test cases, including the linear hydrostatic, linear non-hydrostatic, and Schär mountain. Finally, the new formulation is tested on the baroclinic instability test case on a cubed-sphere mesh.

7.1 Conservation of entropy and total energy

First, we analyze the conservation properties of the newly derived numerical fluxes in the absence of a geopotential term. The semi-discretization is performed via FV method, hence the polynomial degree of DGSEM discretization is zero. A well-known and famous test case to assess PEP property is the density wave, as in [45, 54]. To avoid particular symmetries of the sin function as described in [15], we employ the initial condition

$$(\varrho(x, 0), v(x, 0), p(x, 0)) = (1 + \exp \sin(2\pi x), 1, 1). \quad (162)$$

The solution is computed on the domain $[0, 1]$, over a time interval $[0, 40]$, with a CFL = 0.01. The domain is discretized with 64 cells and periodic boundary conditions are prescribed on the left and right boundaries. The

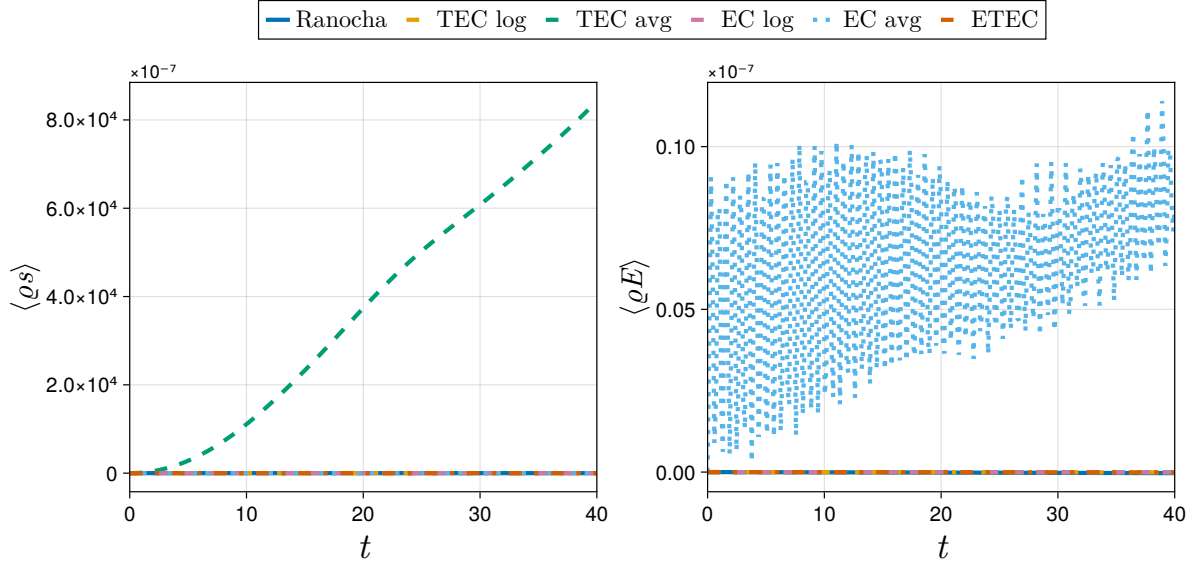


Figure 1: Evolution of the entropy (left) and total energy (right) integrals, normalized with respect to the initial value for the density wave test case using different numerical fluxes and the CFL = 0.01.

EC, TEC and ETEC numerical fluxes for the set of conserved variables $(\varrho, \varrho v, \varrho \theta)$ are compared with different choice of the density mean in the density flux f^e with the EC numerical flux of Ranocha [46] for the conserved variables $(\varrho, \varrho v, \varrho E)$. The evolution of the entropy and total energy integrals can be seen in Figure 1. The entropy conservation results show that the TEC numerical flux is not EC, when the density mean is discretized with the central mean. However, when the logarithmic mean is used, the TEC is able to conserve the entropy up to round-off errors. This can be explained considering that in this test case the velocity v and the pressure p are constants. In fact, the numerical flux for the potential temperature reduces to $f^{\varrho \theta} = \varrho \theta v$ for $p = \text{const}$ and $v = \text{const}$. Thus, recalling Lemma 3.6, the EC condition (25) is satisfied

$$f^e = \{\{\varrho\}\}_{\log} \frac{f^{\varrho \theta}}{\varrho \theta} = \{\{\varrho\}\}_{\log} v. \quad (163)$$

For the conservation of the total energy ϱE , as stated by the Lemma 3.5, all the presented numerical fluxes are TEC for constants p and v . The divergent behaviour of the EC flux with the arithmetic mean for the density in the density flux is due to the lack of PEP property. Indeed, Lemma 3.7 implies that an EC numerical flux with the arithmetic density mean is not PEP. For this reason, in the next sections we will omit the mean value used in the degree freedom of the EC and TEC flux, as it always will be logarithmic mean.

A more involved test case is the three-dimensional inviscid Taylor-Green vortex, which is a canonical benchmark for the transition to turbulence and therefore also the creation of small underresolved scales. The initial conditions are given by [23]

$$\begin{aligned} \varrho(\mathbf{x}, 0) &= 1, \\ u(\mathbf{x}, 0) &= \sin(x) \cos(y) \cos(z), \\ v(\mathbf{x}, 0) &= -\cos(x) \sin(y) \cos(z), \\ w(\mathbf{x}, 0) &= 0, \\ p(\mathbf{x}, 0) &= 10 + \frac{(\cos(2x) + \cos(2y))(\cos(2x) + 2) - 2}{16}. \end{aligned} \quad (164)$$

The solution is computed on the domain $[0, 2\pi]^3$, over a time interval $[0, 50]$, with a CFL = 0.01. The domain is discretized with 32 cells in each direction and periodic boundary conditions are prescribed in each direction. The numerical fluxes ETEC and EC with arithmetic mean and logarithmic mean for the density show numerical

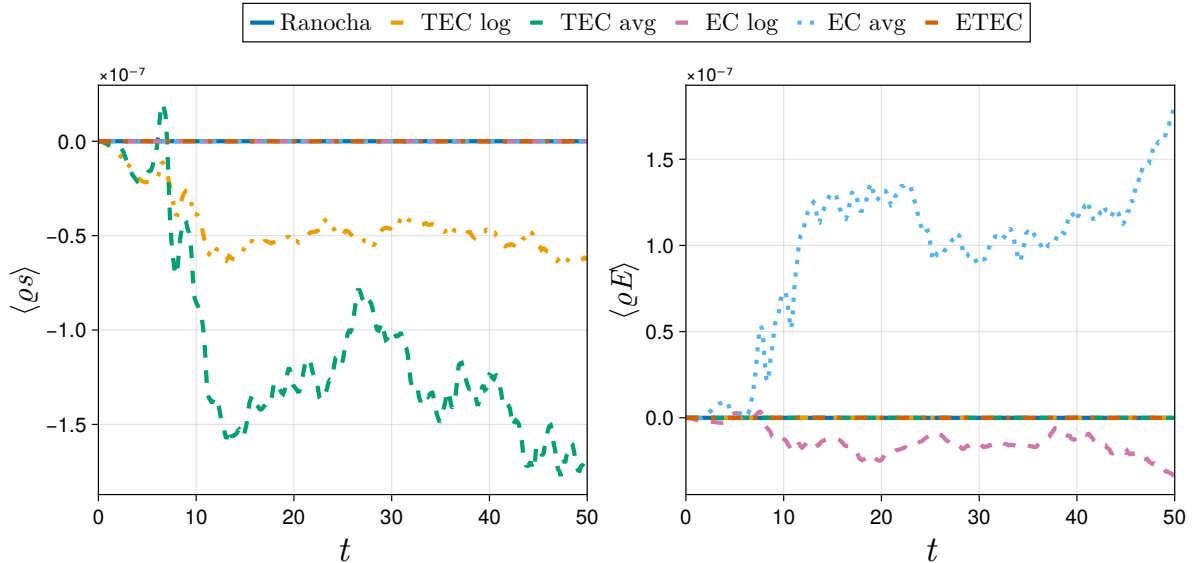


Figure 2: Evolution of the entropy (left) and total energy (right) integrals, normalized with respect to the initial value for the Taylor-Green Vortex test case using different numerical fluxes and the CFL = 0.01.

conservation of the entropy up to round-off errors for long-time simulations. The TEC fluxes clearly are not able to conserve the entropy and the use of a mean over the other does not present any particular benefits. For the conservation of the total energy ϱE , the numerical TEC fluxes with different density mean averages and the ETEC flux are able to conserve the total energy over long simulations.

7.2 Well-balancedness test case

In this section, we assess the well-balancing properties of the proposed numerical fluxes on curvilinear mesh. To this end, we consider two canonical hydrostatic background states: an isothermal atmosphere and a constant potential temperature (adiabatic) atmosphere.

The computational domain is discretized into 16×16 elements, with a polynomial degree of 2. Time integration is carried out with a fixed time step of $\Delta t = 0.01$.

The initial conditions for the isothermal and adiabatic background states are defined as follows. For the isothermal case, the density and pressure fields satisfy the hydrostatic balance under a constant temperature $T_0 = 250$ K, while the velocity field is initially at rest. For the adiabatic atmosphere, the potential temperature $\theta = 300$ K is constant, and the pressure and density are computed to satisfy hydrostatic equilibrium. We employ a smooth curvilinear mapping of the reference coordinates (ξ, η) to physical space (x, y) :

$$x = 500(1 + \xi + 0.1 \sin(\pi\xi) \sin(\pi\eta)), \quad y = 500(1 + \eta + 0.1 \sin(\pi\xi) \sin(\pi\eta)). \quad (165)$$

The warped mesh is shown in Figure 3. The simulations were run up to the final time $T = 5000$ s. In Figures 4 and 5, the L_2 error of the velocity components is shown over the timesteps. Due to the singularity of the logarithmic and Stolarsky mean, a numerically stable evaluation through Taylor expansion is required [29, 64]. These approximations may introduce floating-point errors that accumulate and cause an increase in the error over long integration intervals. Moreover, for the constant potential temperature background state, the growth may occur because floating-point errors trigger a physical instability, as this hydrostatic balance state is metastable. To verify that the growth was solely due to floating-point inaccuracies, we repeated the simulation using 64-bit double precision. The error in the well-balancedness is preserved up to machine precision, even after 500,000 timesteps.

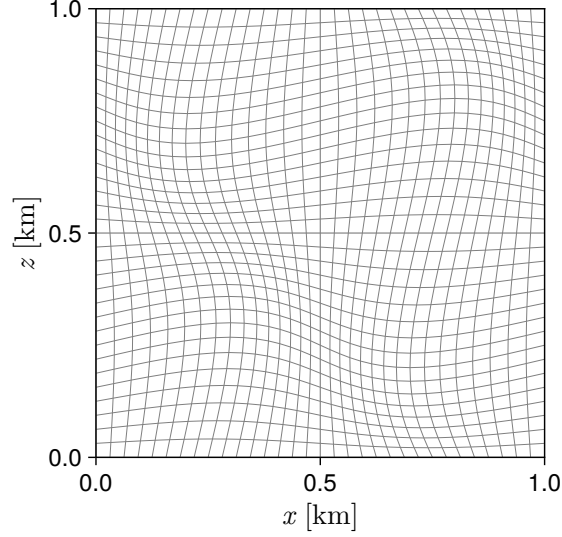


Figure 3: Warped mesh used for well-balancedness test cases.

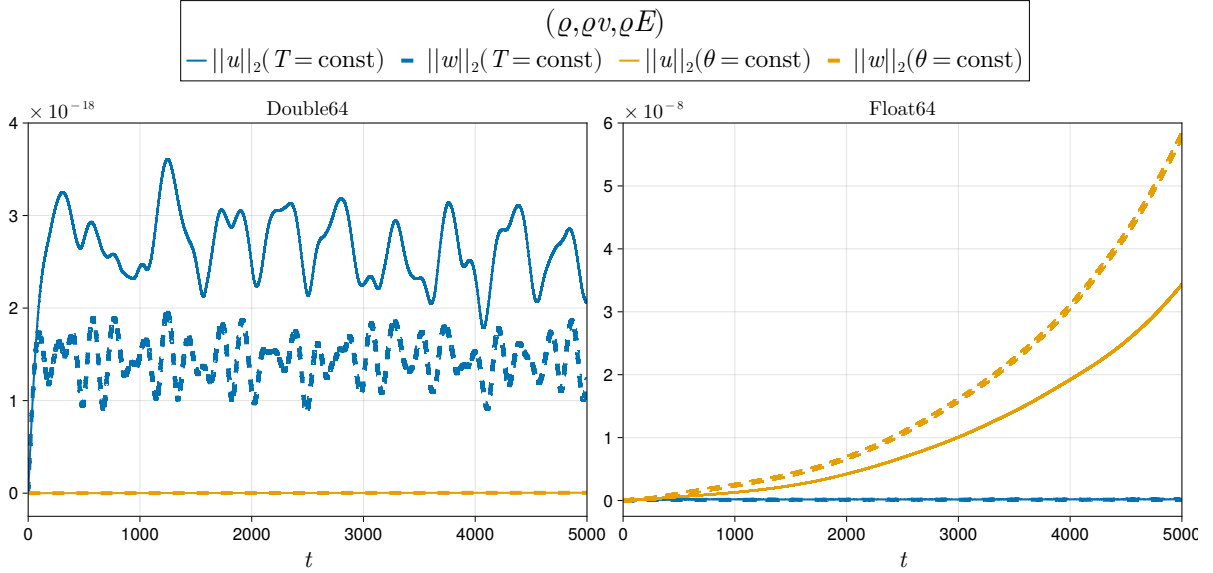


Figure 4: L_2 error of the horizontal and vertical velocity for the two different constant background states for the compressible Euler equation with total energy as prognostic variable.

7.3 Inertia gravity waves

The numerical convergence of the high-order DGSEM can be assessed via the linearized solution obtained by Baldauf et al. [3] for the gravity wave in a channel. The atmosphere is initialized with an isothermal background state with a temperature value of $T_0 = 250$ K. The constant background state is then perturbed with a warm bubble of the form

$$T' = \Delta T \sin\left(\frac{\pi z}{H}\right) \exp\left(-\frac{(x - x_c)^2}{a^2}\right), \quad (166)$$

where ΔT is the maximum temperature perturbation, $H = 10$ km is the height of the channel, $L = 300$ km is the length of the channel, $x_c = 100$ km is the origin of the perturbation, $a = 5$ km is the radius of the bubble perturbation, and x/z are the horizontal/vertical coordinates. The potential $\phi = gz$, where $g = 9.81$ m/s², and the solution is computed from zero to time $t = 1800$ s. The non-conservative flux for both compressible Euler formulations is given by the isothermal well-balanced scheme (91). Several authors [2, 6, 63] have shown that high ΔT leads to saturation error due to the non-linear effects on refined grids and high-order polynomials. Thus,

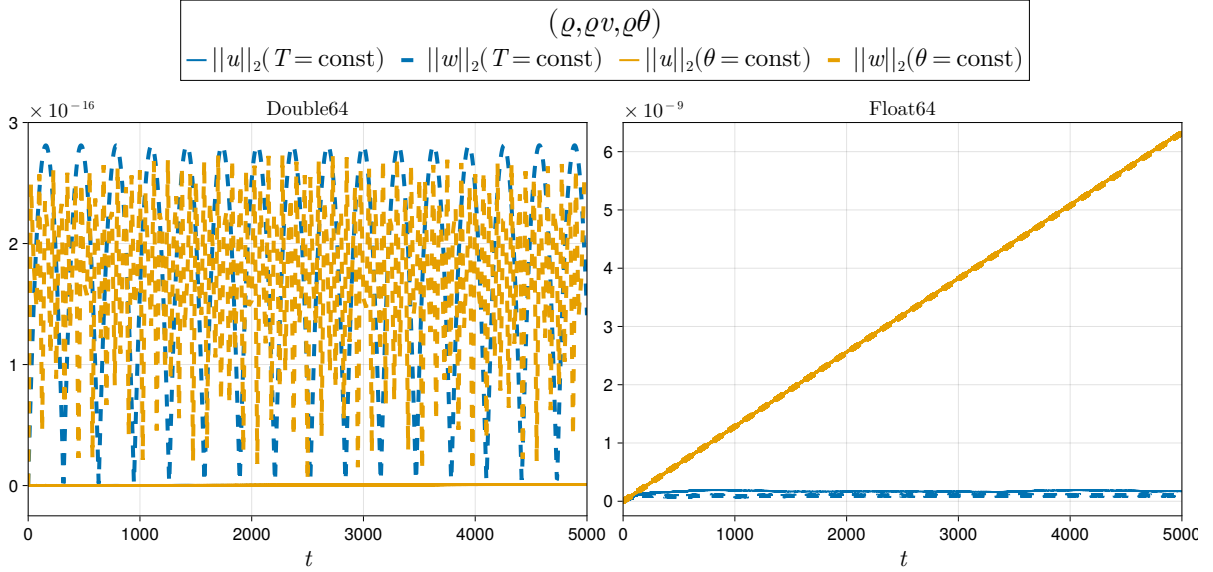


Figure 5: L_2 error of the horizontal and vertical velocity for the two different constant background states for the compressible Euler equation with potential temperature as prognostic variable.

we follow the same approach and set the initial temperature perturbation $\Delta T = 10^{-3}$. The domain is discretized with a uniform grid with $N_x \times N_z$ elements, where the ratio between $\frac{\Delta x}{\Delta z} = 3$ is held constant and the CFL = 0.1.

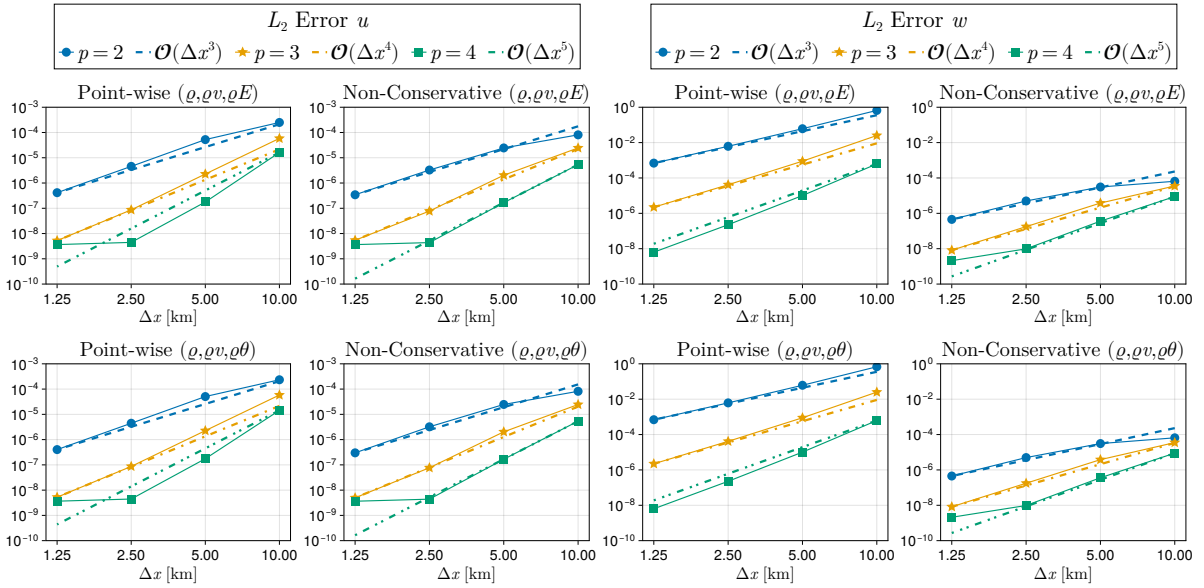


Figure 6: L_2 error of the horizontal (left two columns) and vertical (right two columns) velocity with point-wise (first and third column) and non-conservative (second and fourth column) discretization of the source term, for the Euler equations with total energy (top) and potential temperature (bottom).

Figures 6 show the L_2 errors of the horizontal and vertical velocity components. Our results demonstrate perfect agreement between the two formulations, and in this particular test case, we do not observe a clear advantage of one formulation over the other. We would like to emphasize that the point-wise discretization of the source term, as opposed to the non-conservative approach, shows a difference of four orders of magnitude in the vertical component. This behavior is also observed in the other variables, such as pressure and temperature, reported in Figure 7. Furthermore, the results is in agreement with [63]. Additionally, as in [2, 6, 63], saturation errors arising from nonlinear effects are present for polynomial degree 4, and they are particularly more pronounced in the horizontal velocity component, where it seems to suggest that a plateau has been reached. The analysis has been

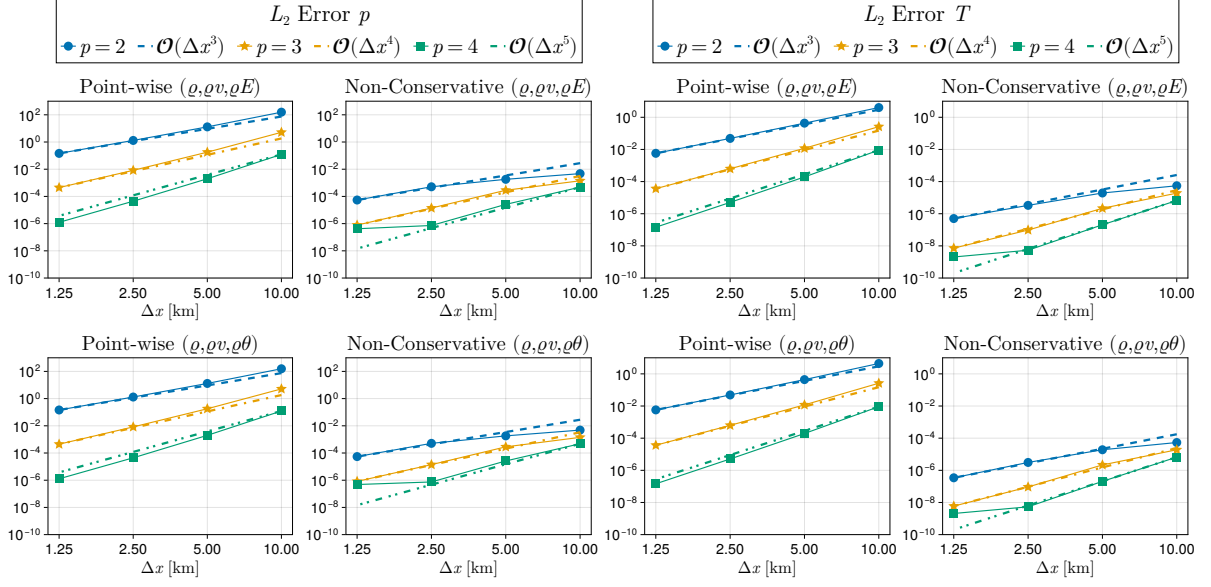


Figure 7: L_2 error of the pressure (left two columns) and temperature (right two columns) with point-wise (first and third column) and non-conservative (second and fourth column) discretization of the source term, for the Euler equations with total energy (top) and potential temperature (bottom).

done also considering the ETEC and EC numerical fluxes for the potential temperature and all the schemes show the same convergence rates.

The numerical fluxes and the two formulations are also compared on curvilinear mesh, with the transformation proposed by [63]. The convergence rates are shown in Figure 8. Compared to the point-wise discretization, the non-conservative discretization shows significantly lower error due to the extension of the well-balanced property to curvilinear meshes.

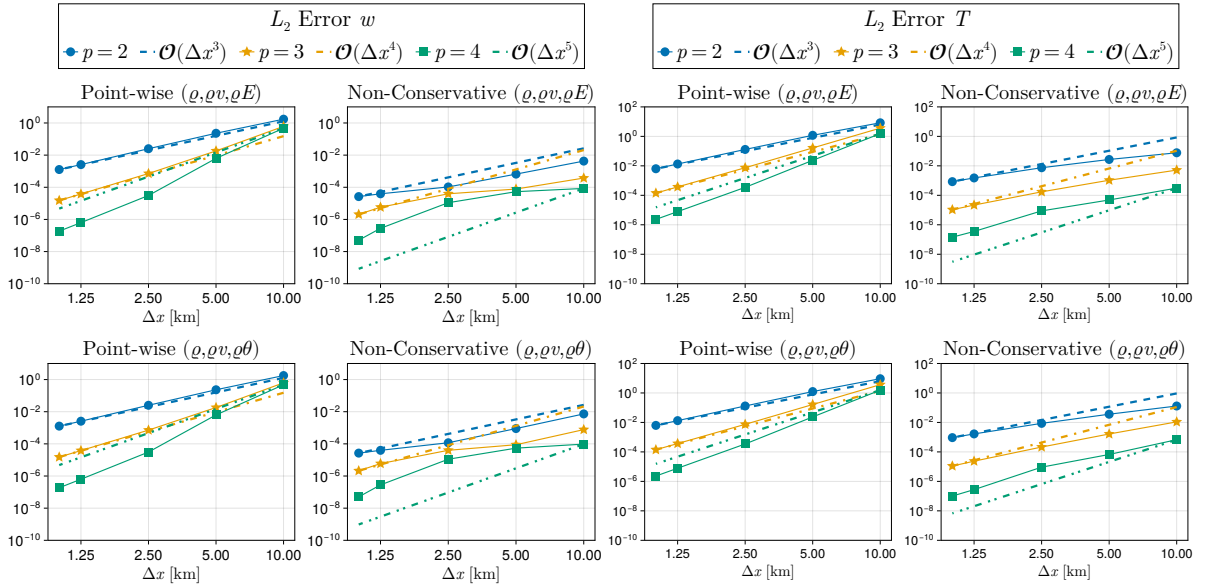


Figure 8: L_2 error of the vertical velocity (left two columns) and temperature (right two columns) with point-wise (first and third column) and non-conservative (second and fourth column) discretization of the source term, for the Euler equations with total energy (top) and potential temperature (bottom) on the warped mesh.

The convergence analysis has also been conducted with different numerical fluxes for the source term and having the well-balanced scheme appears to be crucial for high-order convergence of the solution, in contrast to conservation of TEC and KPEP, which play a marginal role in this particular test case. Figure 9 shows a contour

comparison between the point-wise and non-conservative discretization. The oscillations observed in the point-wise source term discretization are purely numerical, resulting from the lack of a well-balanced scheme.

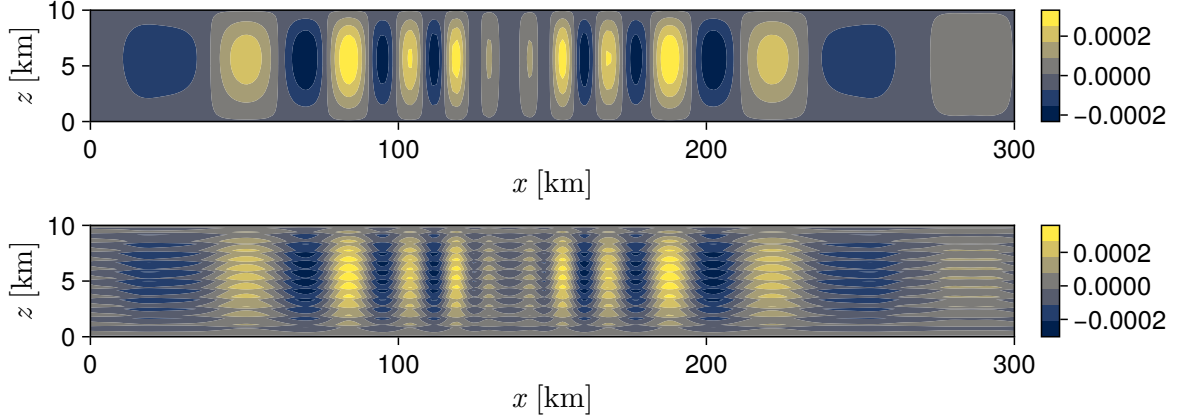


Figure 9: Contour of the vertical velocity with non-conservative (top panel) and point-wise (bottom panel) discretization of the source term, for the Euler equations with potential temperature.

7.4 Numerical results with orography

In this section we present the numerical results for three idealized flows over orography. To avoid spurious and unphysical solutions due to the reflections on the domain extrema, non-reflecting boundary conditions are prescribed on the top and lateral boundaries, with the introduction of Rayleigh damping profiles as in [25, 40], which we provide here for completeness. On the right-hand side of the momentum and either total energy or potential temperature equation, we add the source terms

$$\begin{aligned} \mathbf{q}_V &= \varrho(\mathbf{V} - \mathbf{V}^0)(S_V + S_{h_1} + S_{h_2}), \\ q_{\theta} &= \varrho(\theta - \theta^0)(S_V + S_{h_1} + S_{h_2}), \\ q_{\varrho E} &= \varrho(\theta - \theta^0)K \frac{\gamma}{\gamma - 1} (\varrho\theta)^{\gamma-1} (S_V + S_{h_1} + S_{h_2}) + \mathbf{V} \cdot \mathbf{q}_V, \end{aligned} \quad (167)$$

where the Rayleigh damping profiles S_u , S_{h_1} , and S_{h_2} are defined as

$$\begin{aligned} S_v &= \begin{cases} 0, & \text{if } z < z_B \\ \alpha \sin^2 \left[\frac{\pi}{2} \left(\frac{z - z_B}{z_T - z_B} \right) \right], & \text{if } z \geq z_B \end{cases} \\ S_{h_1} &= \begin{cases} 0, & \text{if } x < x_B \\ \alpha \sin^2 \left[\frac{\pi}{2} \left(\frac{x - x_B}{x_T - x_B} \right) \right], & \text{if } x \geq x_B \end{cases} \\ S_{h_2} &= \begin{cases} 0, & \text{if } x > -x_B \\ \alpha \sin^2 \left[\frac{\pi}{2} \left(\frac{x + x_B}{x_B - x_T} \right) \right], & \text{if } x \leq -x_B. \end{cases} \end{aligned} \quad (168)$$

7.4.1 Linear hydrostatic mountain

The first classical benchmark test case of a flow over a hill is the linear hydrostatic mountain, see [18, 24] for a thorough description of the test case. The mountain profile is the well-known *versiera di Agnesi* given by

$$h(x, z) = \frac{h_c}{1 + \left(\frac{x}{a_c} \right)^2}, \quad (169)$$

where h_c is the height of the mountain and a_c is its half-width. The computational domain is $[-120, 120] \times [0, 30]$ km², thus the mountain peak is centered at 0 with $h_c = 1$ m and $a_c = 10$ km. The atmosphere is initialized with a constant background temperature $T_0 = 250$ K and a constant mean flow $\bar{u} = 20$ km. The pressure is initialized with the Exner pressure $\bar{\pi}$ with the following $p = p_0 \bar{\pi}^{c_p/R}$, where $\bar{\pi} = \exp(\mathcal{N}^2/gz)$ and $\mathcal{N} =$

$g/\sqrt{c_p T_0}$ is the Brunt-Väisälä frequency. Since in this case $\frac{N_{ac}}{\bar{u}} > 1$, the flow is in hydrostatic regime [24, 41]. A no-slip boundary condition is used at the bottom and non-reflecting boundary conditions are used at the top and lateral boundaries, with $\alpha = 0.1$, $z_B = 15$ km, $z_T = 30$ km, $x_B = 80$ km, and $x_T = 120$ km. The polynomial degree is $p = 3$ and, and we use 100×60 elements (horizontal \times vertical direction).

The quantity of interest for this benchmark is the analytical momentum flux [56]

$$m = \int_{-\infty}^{\infty} \bar{\rho}(z) u'(x, z) w'(x, z) dx, \quad (170)$$

where u' and w' are the velocity perturbations and $\bar{\rho}$ is the density. The analytical momentum flux is given by

$$m^H = -\frac{\pi}{4} \bar{\rho}_s \bar{u}_s N h_m^2, \quad (171)$$

where $\bar{\rho}_s$ and \bar{u}_s are the background surface density and velocity. Thus, the ratio m/m^H has to be as close as possible to 1. Figure 10 shows the normalized momentum for both formulations with different discretizations of the source terms. The non-conservative formulations show the same results for both sets of conserved variables and an increased robustness compared to the point-wise discretization of the source term, which shows spurious oscillations. This behavior can also be seen in Figure 11, where the evolution of the normalized momentum is reported. It can be noticed that while the momentum approaches its analytical value, for the non-conservative formulations there are no spurious oscillations. Figure 12 shows the contour plots of the horizontal and vertical velocity components. On a more refined grid the two schemes for both sets of conserved variables agree rather well and the spurious oscillations diminish (here not shown).

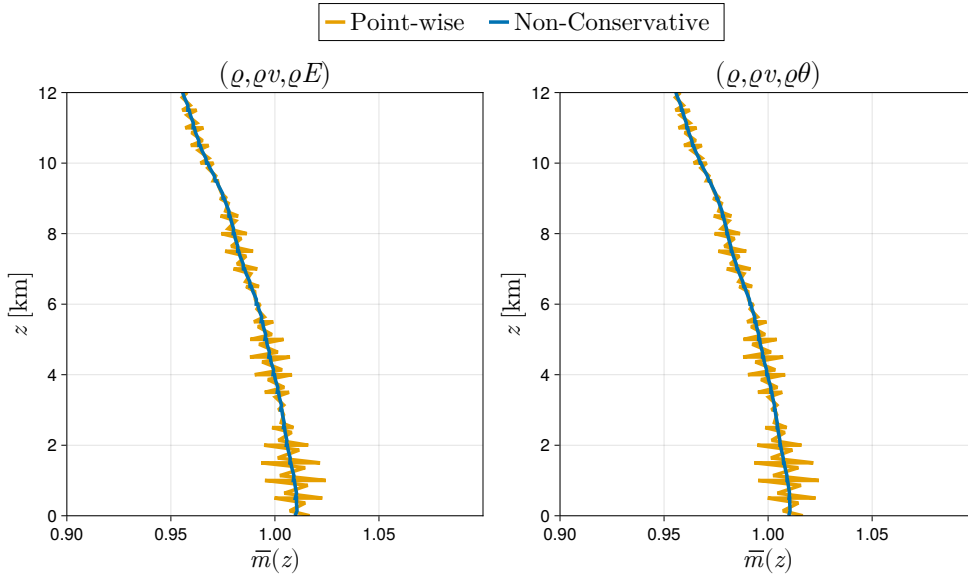


Figure 10: Comparison of the normalized momentum for the linear hydrostatic mountain test case for the 4 different formulations at $T = 12.5$ h, with 100×60 elements along the x direction and z direction, respectively, and $p = 3$.

7.4.2 Linear nonhydrostatic mountain

The second classical benchmark test case focuses on linear nonhydrostatic mountain waves, see [18, 24] for a detailed description of the test case. Here, the initial atmospheric state consists of a uniform horizontal mean flow $\bar{u} = 10$ m/s within a uniformly stratified atmosphere characterized by a constant Brunt-Väisälä frequency $\mathcal{N} = 0.01$ s $^{-1}$. The potential temperature and Exner pressure profiles are initialized following the hydrostatic balance:

$$\bar{\pi}(z) = 1 + \frac{g^2}{c_p \theta_0 \mathcal{N}^2} \left(\exp\left(-\frac{\mathcal{N}^2}{g} z\right) - 1 \right), \quad (172)$$

where $\theta_0 = 280$ K is the surface potential temperature. The pressure is computed as

$$p = p_0 \bar{\pi}^{c_p/R}, \quad (173)$$

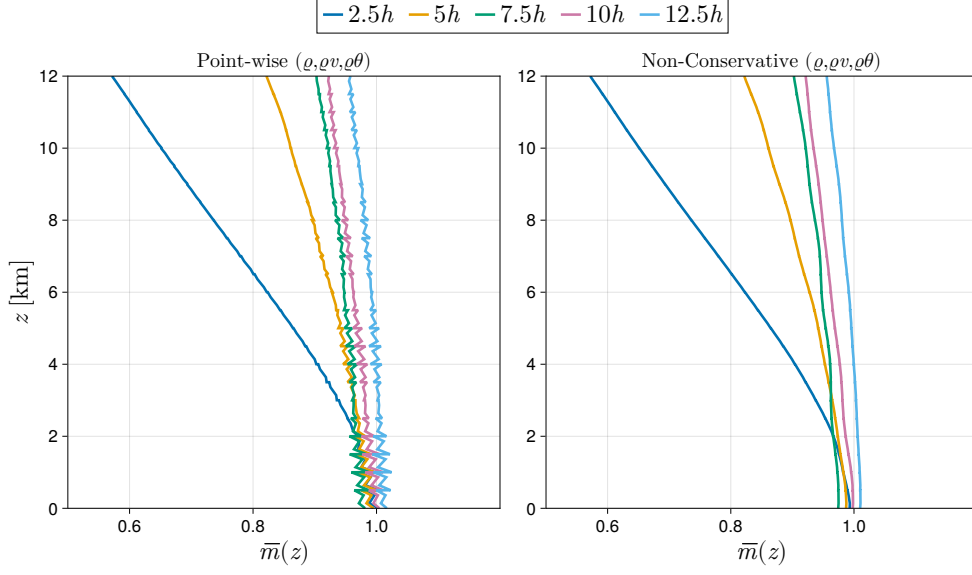


Figure 11: Evolution of the normalized momentum for the linear hydrostatic mountain with 100×60 elements along the x and z direction respectively and $p = 3$.

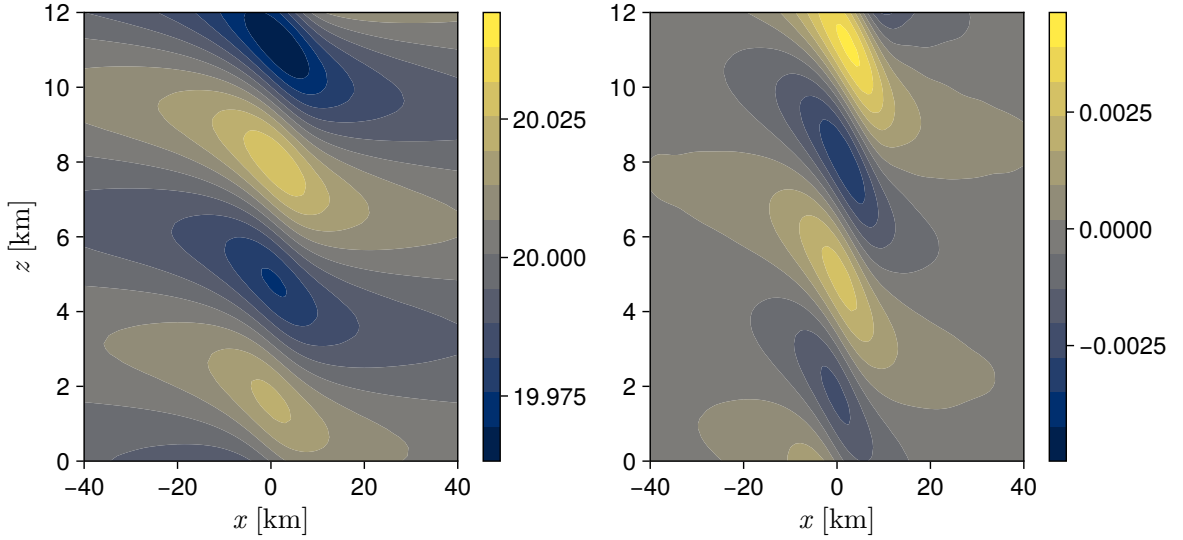


Figure 12: Contour of the horizontal (left) and vertical (right) velocity components for the linear hydrostatic mountain with 100×60 elements along the x and z direction respectively and $p = 3$.

where $R = c_p - c_v$ is the gas constant for dry air. The potential temperature is given by

$$\theta(z) = \theta_0 \exp\left(\frac{N^2}{g}z\right), \quad (174)$$

and the temperature is recovered by $T = \theta\bar{\pi}$. The background density is

$$\bar{\rho} = \frac{p}{RT}. \quad (175)$$

The initial velocity field is set as $u = \bar{u}$ and $w = 0$. The mountain profile is given by the classical *versiera di Agnesi* (169), where $h_c = 1$ m is the mountain height and $a_c = 1$ km is the half-width.

The computational domain is $(x, z) \in [0, 144] \times [0, 30]$ km², and the simulation time spans $t \in [0, 8]$ hours. No-flux boundary conditions are imposed at the bottom, while non-reflecting boundary conditions are used at the top and lateral boundaries. Damping layers are applied in the last 15 km in the vertical direction and over the last 40 km in the horizontal direction, with a damping coefficient $\alpha = 0.03$.

Since in this configuration $\mathcal{N}a_c/\bar{u} = 1$, the flow is in the nonhydrostatic regime [24, 41]. The quantity of interest for this benchmark is again the normalized momentum flux, defined analogously to the hydrostatic test case and normalized by $m^{NH} = 0.457m^H$ [32]. The results for the linear nonhydrostatic mountain test case are shown in Figures 13 and 14. The normalized momentum flux, computed at $T = 8$ h and reported in Figure 13, approaches the theoretical value of 1 for all formulations, similarly to what was observed in the hydrostatic case.

Figure 14 visualizes the time evolution of the normalized momentum, showing values plotted at times 2 h, 4 h, 6 h, and 8 h. It can be observed that the normalized momentum progressively approaches the expected value of 1 over time. However, spurious oscillations are present, especially for the point-wise discretization of the source terms. These oscillations are less pronounced when using the non-conservative formulation, indicating a more robust behavior. Figure 15 shows contour plots of the horizontal and vertical velocity components.

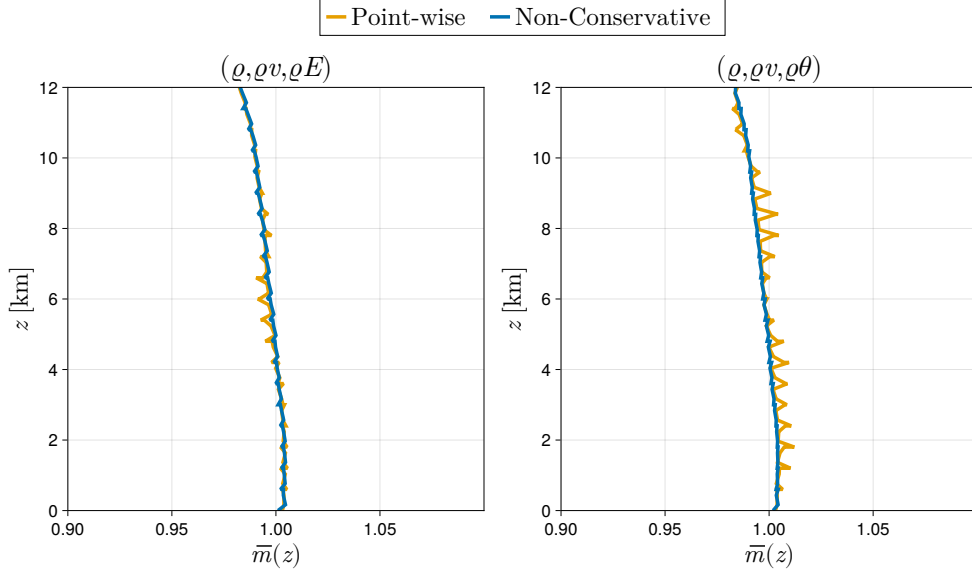


Figure 13: Comparison of the normalized momentum for the linear nonhydrostatic mountain test case for the 4 different formulations at $T = 8$ h, with 200×50 elements along the x direction and z direction, respectively, and $p = 3$.

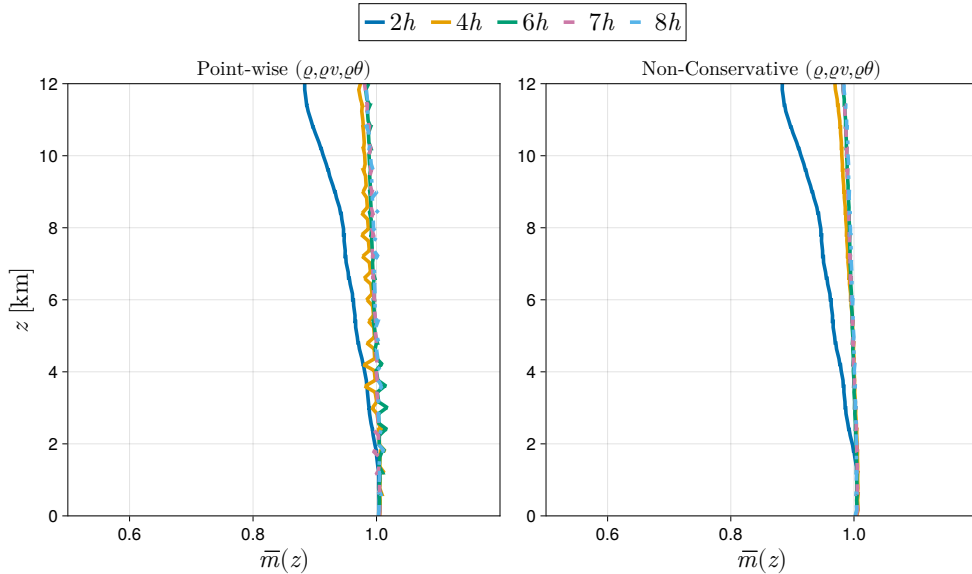


Figure 14: Evolution of the normalized momentum for the linear nonhydrostatic mountain with 200×50 elements along the x and z direction respectively and $p = 3$.

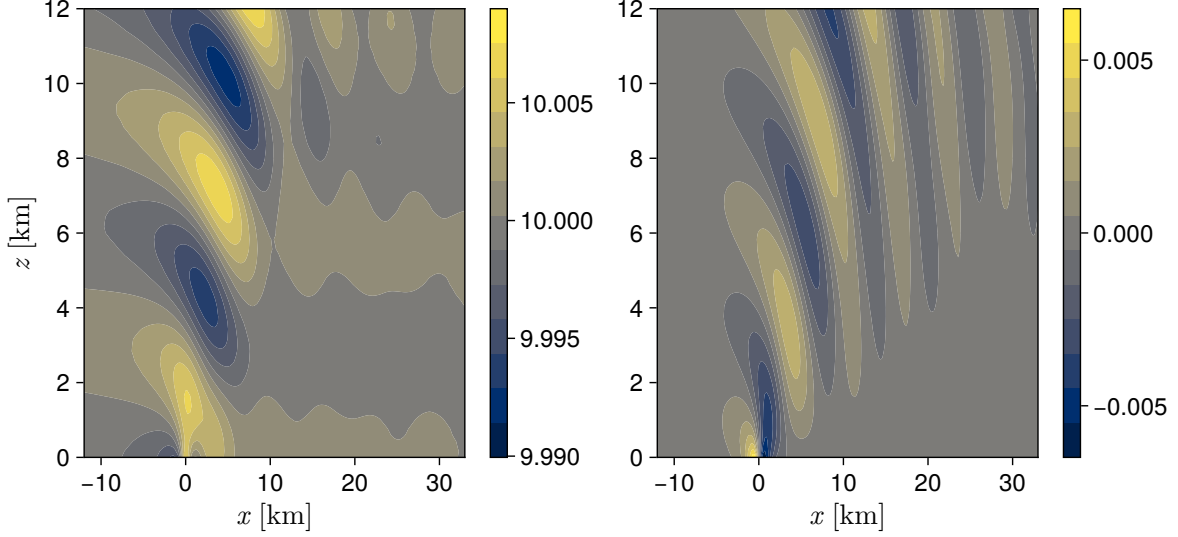


Figure 15: Contour of the horizontal (left) and vertical (right) velocity components for the linear nonhydrostatic mountain with 200×50 elements along the x and z direction respectively and $p = 3$.

7.4.3 Schär mountain

The third benchmark test case considers the steady-state hydrostatic flow over an idealized multi-peak mountain, known as the Schär mountain [53]. The mountain profile is defined by

$$h(x) = h_c \exp\left(-\left(\frac{x}{a_c}\right)^2\right) \cos^2\left(\pi \frac{x}{\lambda_c}\right), \quad (176)$$

where $h_c = 250$ m is the maximum mountain height, $a_c = 5000$ m controls the width of the Gaussian envelope, and $\lambda_c = 4000$ m sets the wavelength of the cosine perturbation. The resulting orography generates five mountain peaks, symmetrically distributed around the domain center.

The computational domain is $[-25\,000, 25\,000] \times [0, 21\,000]$ m², with a simulation time interval $t \in [0, 10]$ h. No-flux boundary conditions are imposed at the bottom, while non-reflecting boundary conditions are enforced at the top and lateral boundaries using Rayleigh damping layers. Specifically, sponge layers are applied in the last 8 km of the vertical direction and in the last 5 km near both lateral boundaries, with a damping coefficient $\alpha = 0.03$.

The atmosphere is initialized with a uniform horizontal mean flow $\bar{u} = 10$ m/s and a constant Brunt-Väisälä frequency $\mathcal{N} = 0.01$ s⁻¹. The initial thermodynamic profiles are derived under the assumption of hydrostatic balance. The Exner pressure $\bar{\pi}(z)$ is given by

$$\bar{\pi}(z) = 1 + \frac{g^2}{c_p \theta_0 \mathcal{N}^2} \left(\exp\left(-\frac{\mathcal{N}^2}{g} z\right) - 1 \right), \quad (177)$$

where $\theta_0 = 280$ K is the reference potential temperature at the surface. The pressure is then initialized as

$$p = p_0 \bar{\pi}^{c_p/R}, \quad (178)$$

with reference pressure $p_0 = 10\,000$ Pa and gas constant $R = c_p - c_v$ for dry air. The potential temperature evolves with height as

$$\theta(z) = \theta_0 \exp\left(\frac{\mathcal{N}^2}{g} z\right), \quad (179)$$

and the temperature is computed as $T(z) = \theta(z)\bar{\pi}(z)$. The corresponding background density profile is given by the ideal gas law

$$\bar{\varrho}(z) = \frac{p(z)}{RT(z)}. \quad (180)$$

The initial velocity field is set uniformly as $u = \bar{u}$ and $w = 0$.

Since in this configuration $\mathcal{N}a_c/\bar{u} > 1$, the flow is (strongly) non-hydrostatic [24, 53]. Figure 16 shows the contour of the horizontal and vertical velocity components at $T = 5$ h. For this particular test case, the two formulations and the two discretization are in good agreement.

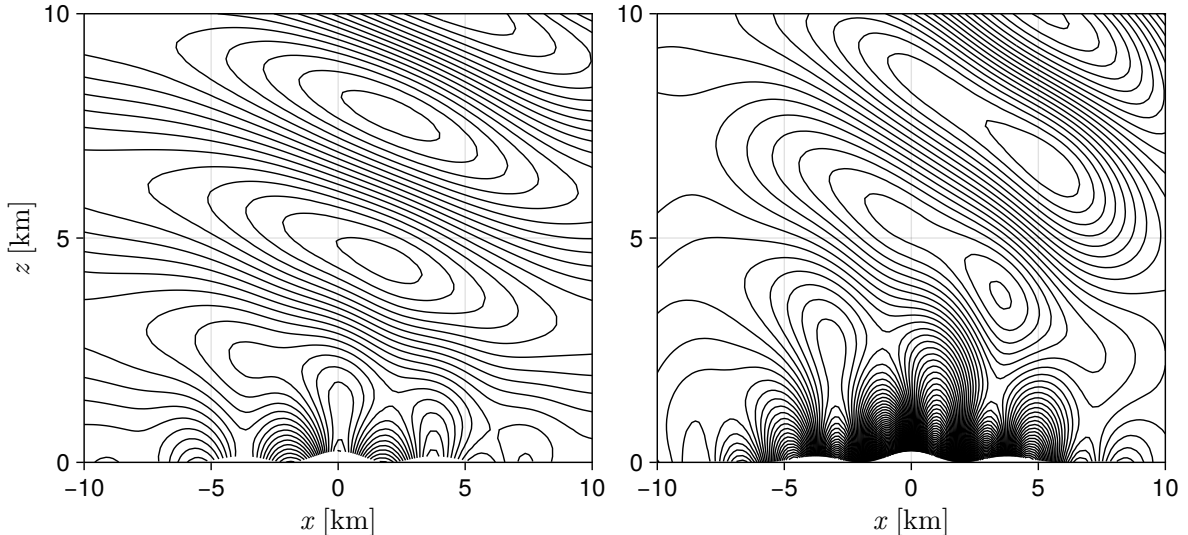


Figure 16: Contour lines of the horizontal (left) and vertical (right) velocity perturbation components for the mountain Schär test case with 100×50 elements along the x and z direction respectively and $p = 3$. Contour values are between -2 m/s and 2 m/s with an interval equal to 0.2 m/s for horizontal velocity component and between -2 m/s and 2 m/s with an interval equal to 0.05 m/s for vertical velocity component.

7.5 Baroclinic instability

To further validate our formulation, we employ the baroclinic wave benchmark originally formulated by Ullrich et al. [61] and adopted in the 2016 edition of the Dynamical Core Model Intercomparison Project (DCMIP) [60]. This configuration has become a standard test for assessing the ability of atmospheric models to reproduce midlatitude baroclinic instability.

The initial state is a balanced, axisymmetric solution of the deep-atmosphere equations, as described in Appendix A of Ullrich et al. [61]. A localized Gaussian perturbation is applied to the zonal wind field in the northern midlatitudes, which excites the growth of a baroclinic disturbance. In the early stages (up to about day 7) the evolution is predominantly linear, while at later times nonlinear interactions lead to steepening and eventual wave breaking.

In our study the simulation length is set to 10 days, covering both the linear growth phase and the transition to nonlinearity. The spatial discretization uses an equiangular cubed-sphere grid with $K_h = 8$ elements on the horizontal and $K_v = 4$ elements in the vertical, for a total of six panels and polynomial degree $p = 5$.

The point-wise discretization of the source term is unconditionally unstable, independently by the set of equations. On the other hand the non-conservative formulation could run stably and without any need of filtering for long simulation time. The contour of the surface pressure after 10 days are shown in Figure 17.

8 Conclusions

In this work we derived three new numerical fluxes for the compressible Euler equations, formulated with potential temperature as a primary invariant. Depending on the choice, these fluxes can preserve thermodynamic entropy (EC), total energy (TEC), or both simultaneously (ETEC). The EC and TEC fluxes allow a degree of freedom in the density flux. For both cases, the logarithmic mean provide the most robust formulation; the EC flux then is PEP, while the TEC flux additionally satisfies the EC condition under constant pressure. We introduced a general definition of the kinetic and potential energy preservation (KPEP) property and derived a condition for total energy conservation (TEC), when a geopotential term is included, which rely on a non-conservative discretization of the geopotential term in flux differencing form. Furthermore, we developed a well-balanced scheme for the case of a constant background potential temperature and extended all properties to discontinuous Galerkin spectral-element method (DGSEM) on arbitrary curvilinear coordinates. The robustness and accuracy of the novel numerical fluxes and schemes have been assessed with a variety of standard atmospheric benchmark problems. The correct convergence rates were obtained, and the non-conservative approach showed up to two to four order of magnitude improvement, where the well-balancedness property was crucial to achieving such differences. The numerical experiments demonstrated that the newly derived fluxes are both robust and accurate, performing consistently with

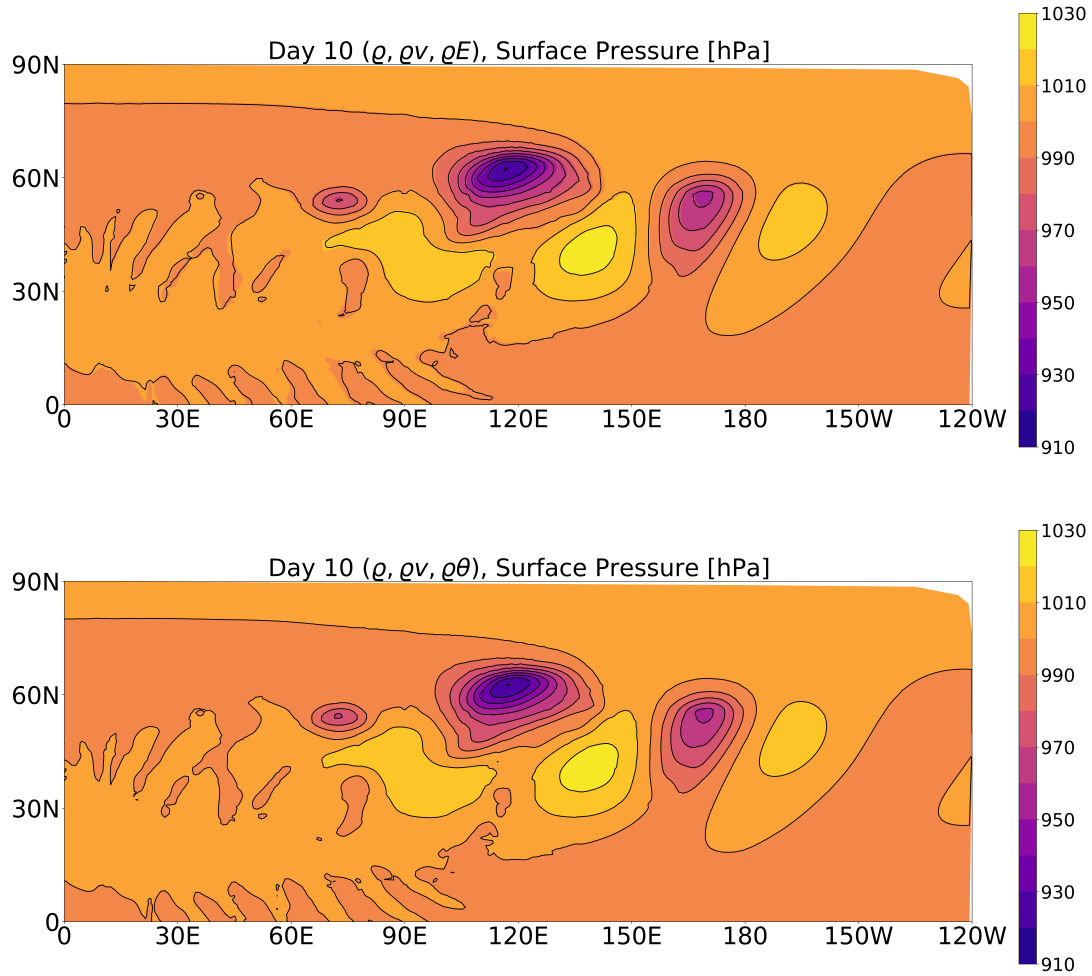


Figure 17: Contour of the surface pressure at day 10 for the baroclinic instability test case, with polynomial degree 5.

the entropy conservative Ranocha flux for the total energy formulation. No significant differences were observed between the two formulations, using total energy or potential temperature as prognostic variables, indicating that neither approach appears to offer a clear advantage over the other based on our test cases. Additionally, schemes employing a non-conservative discretization of the source term consistently exhibited higher robustness and accuracy compared to the point-wise approach.

Acknowledgments

This work was supported by the Max Planck Graduate Center with the Johannes Gutenberg University of Mainz (MPGC). MA and HR were supported by the Deutsche Forschungsgemeinschaft (DFG, German Research Foundation, project numbers 513301895 and 528753982 as well as within the DFG priority program SPP 2410 with project number 526031774) and the Daimler und Benz Stiftung (Daimler and Benz foundation, project number 32-10/22). We acknowledge support from the Mainz Institute of Multiscale Modeling (M3ODEL).

We thank Andrés Rueda-Ramírez for some valuable discussions on well-balanced methods and structure-preserving discretizations.

Data availability statement

All Julia source code and data needed to reproduce the numerical results presented in this paper are available in our reproducibility repository [1].

References

- [1] M. Artiano, O. Knoth, P. Spichtinger, and H. Ranocha. *Reproducibility repository for "Structure-Preserving High-Order Methods for the Compressible Euler Equations in Potential Temperature Formulation for Atmospheric Flows"*. https://github.com/MarcoArtiano/2025_structure_potential_temperature. 2025. DOI: TODO.
- [2] M. Baldauf. "A horizontally explicit, vertically implicit (HEVI) discontinuous Galerkin scheme for the 2-dimensional Euler and Navier-Stokes equations using terrain-following coordinates". In: *Journal of Computational Physics* 446 (2021), p. 110635. DOI: 10.1016/j.jcp.2021.110635.
- [3] M. Baldauf and S. Brdar. "An analytic solution for linear gravity waves in a channel as a test for numerical models using the non-hydrostatic, compressible Euler equations". In: *Quarterly Journal of the Royal Meteorological Society* 139.677 (2013), pp. 1977–1989. DOI: 10.1002/qj.2105.
- [4] T. J. Barth. "Numerical Methods for Gasdynamic Systems on Unstructured Meshes". In: *An Introduction to Recent Developments in Theory and Numerics for Conservation Laws: Proceedings of the International School on Theory and Numerics for Conservation Laws, Freiburg/Littenweiler, October 20–24, 1997*. Ed. by D. Kröner, M. Ohlberger, and C. Rohde. Berlin, Heidelberg: Springer Berlin Heidelberg, 1999, pp. 195–285. DOI: 10.1007/978-3-642-58535-7_5.
- [5] J. Bezanson, A. Edelman, S. Karpinski, and V. B. Shah. "Julia: A Fresh Approach to Numerical Computing". In: *SIAM Review* 59.1 (2017), pp. 65–98. DOI: 10.1137/141000671.
- [6] S. Blaise, J. Lambrechts, and E. Deleersnijder. "A stabilization for three-dimensional discontinuous Galerkin discretizations applied to nonhydrostatic atmospheric simulations". In: *International Journal for Numerical Methods in Fluids* 81.9 (2016), pp. 558–585. DOI: 10.1002/flid.4197.
- [7] M. Bohm, A. R. Winters, G. J. Gassner, D. Derigs, F. Hindenlang, and J. Saur. "An entropy stable nodal discontinuous Galerkin method for the resistive MHD equations. Part I: Theory and numerical verification". In: *Journal of Computational Physics* 422 (2020), p. 108076. DOI: <https://doi.org/10.1016/j.jcp.2018.06.027>.
- [8] M. H. Carpenter, T. C. Fisher, E. J. Nielsen, and S. H. Frankel. "Entropy Stable Spectral Collocation Schemes for the Navier–Stokes Equations: Discontinuous Interfaces". In: *SIAM Journal on Scientific Computing* 36.5 (2014), B835–B867. DOI: 10.1137/130932193.
- [9] M. H. Carpenter, M. Parsani, E. J. Nielsen, and T. C. Fisher. "Towards an Entropy Stable Spectral Element Framework for Computational Fluid Dynamics". In: *54th AIAA Aerospace Sciences Meeting*. DOI: 10.2514/6.2016-1058.
- [10] P. Chandrashekar. "Kinetic Energy Preserving and Entropy Stable Finite Volume Schemes for Compressible Euler and Navier-Stokes Equations". In: *Communications in Computational Physics* 14 (Sept. 2012). DOI: 10.4208/cicp.170712.010313a.
- [11] P. Chandrashekar and C. Klingenberg. "A Second Order Well-Balanced Finite Volume Scheme for Euler Equations with Gravity". In: *SIAM Journal on Scientific Computing* 37.3 (2015), B382–B402. DOI: 10.1137/140984373.
- [12] H. Chen. "Means Generated by an Integral". In: *Mathematics Magazine* 78.5 (2005), pp. 397–399. DOI: 10.2307/30044201.
- [13] X. Chen, N. Andronova, B. V. Leer, J. E. Penner, J. P. Boyd, C. Jablonowski, and S.-J. Lin. "A Control-Volume Model of the Compressible Euler Equations with a Vertical Lagrangian Coordinate". In: *Monthly Weather Review* 141.7 (2013), pp. 2526–2544. DOI: 10.1175/MWR-D-12-00129.1.
- [14] S. Danisch and J. Krumbiegel. "Makie.jl: Flexible high-performance data visualization for Julia". In: *Journal of Open Source Software* 6.65 (2021), p. 3349. DOI: 10.21105/joss.03349.
- [15] C. De Michele and G. Coppola. "Asymptotically entropy-conservative and kinetic-energy preserving numerical fluxes for compressible Euler equations". In: *Journal of Computational Physics* 492 (2023), p. 112439. DOI: 10.1016/j.jcp.2023.112439.
- [16] D. Derigs, A. R. Winters, G. J. Gassner, and S. Walch. "A novel averaging technique for discrete entropy-stable dissipation operators for ideal MHD". In: *Journal of Computational Physics* 330 (2017), pp. 624–632. DOI: 10.1016/j.jcp.2016.10.055.
- [17] D. Derigs, A. R. Winters, G. J. Gassner, S. Walch, and M. Bohm. "Ideal GLM-MHD: About the entropy consistent nine-wave magnetic field divergence diminishing ideal magnetohydrodynamics equations". In: *Journal of Computational Physics* 364 (2018), pp. 420–467. DOI: 10.1016/j.jcp.2018.03.002.

- [18] D. R. Durran and J. B. Klemp. “A Compressible Model for the Simulation of Moist Mountain Waves”. In: *Monthly Weather Review* 111.12 (1983), pp. 2341–2361. DOI: 10.1175/1520-0493(1983)111<2341:ACMFTS>2.0.CO;2.
- [19] T. C. Fisher and M. H. Carpenter. “High-order entropy stable finite difference schemes for nonlinear conservation laws: Finite domains”. In: *Journal of Computational Physics* 252 (2013), pp. 518–557. DOI: 10.1016/j.jcp.2013.06.014.
- [20] U. S. Fjordholm, S. Mishra, and E. Tadmor. “Well-balanced and energy stable schemes for the shallow water equations with discontinuous topography”. In: *Journal of Computational Physics* 230.14 (2011), pp. 5587–5609. DOI: <https://doi.org/10.1016/j.jcp.2011.03.042>.
- [21] G. J. Gassner, A. R. Winters, and D. A. Kopriva. “A well balanced and entropy conservative discontinuous Galerkin spectral element method for the shallow water equations”. In: *Applied Mathematics and Computation* 272 (2016). Recent Advances in Numerical Methods for Hyperbolic Partial Differential Equations, pp. 291–308. DOI: 10.1016/j.amc.2015.07.014.
- [22] G. J. Gassner. “A Skew-Symmetric Discontinuous Galerkin Spectral Element Discretization and Its Relation to SBP-SAT Finite Difference Methods”. In: *SIAM Journal on Scientific Computing* 35.3 (2013), A1233–A1253. DOI: 10.1137/120890144.
- [23] G. J. Gassner, A. R. Winters, and D. A. Kopriva. “Split Form Nodal Discontinuous Galerkin Schemes with Summation-By-Parts Property for the Compressible Euler Equations”. In: *Journal of Computational Physics* 327 (2016), pp. 39–66. DOI: 10.1016/j.jcp.2016.09.013.
- [24] F. Giraldo and M. Restelli. “A study of spectral element and discontinuous Galerkin methods for the Navier–Stokes equations in nonhydrostatic mesoscale atmospheric modeling: Equation sets and test cases”. In: *Journal of Computational Physics* 227.8 (2008), pp. 3849–3877. DOI: 10.1016/j.jcp.2007.12.009.
- [25] M. Girfoglio, A. Quaini, and G. Rozza. “A comparative computational study of different formulations of the compressible Euler equations for mesoscale atmospheric flows in a finite volume framework”. In: *Computers & Fluids* 288 (2025), p. 106510. DOI: 10.1016/j.compfluid.2024.106510.
- [26] E. Godlewski and P.-A. Raviart. *Numerical Approximation of Hyperbolic Systems of Conservation Laws*. Vol. 72. Texts in Applied Mathematics. Springer, 2021. DOI: 10.1007/978-1-0716-1344-3.
- [27] S. Gottlieb, D. I. Ketcheson, and C.-W. Shu. *Strong stability preserving Runge-Kutta and multistep time discretizations*. Singapore: World Scientific, 2011.
- [28] J. D. Hunter. “Matplotlib: A 2D graphics environment”. In: *Computing in Science & Engineering* 9.3 (2007), pp. 90–95. DOI: 10.1109/MCSE.2007.55.
- [29] F. Ismail and P. L. Roe. “Affordable, entropy-consistent Euler flux functions II: Entropy production at shocks”. In: *Journal of Computational Physics* 228.15 (2009), pp. 5410–5436. DOI: 10.1016/j.jcp.2009.04.021.
- [30] A. Jameson. “Formulation of Kinetic Energy Preserving Conservative Schemes for Gas Dynamics and Direct Numerical Simulation of One-Dimensional Viscous Compressible Flow in a Shock Tube Using Entropy and Kinetic Energy Preserving Schemes”. In: *Journal of Scientific Computing* 34.2 (2008), pp. 188–208. DOI: 10.1007/s10915-007-9172-6.
- [31] C. A. Kennedy and A. Gruber. “Reduced aliasing formulations of the convective terms within the Navier–Stokes equations for a compressible fluid”. In: *Journal of Computational Physics* 227.3 (2008), pp. 1676–1700. DOI: 10.1016/j.jcp.2007.09.020.
- [32] J. B. Klemp and D. R. Durran. “An Upper Boundary Condition Permitting Internal Gravity Wave Radiation in Numerical Mesoscale Models”. In: *Monthly Weather Review* 111.3 (1983), pp. 430–444. DOI: 10.1175/1520-0493(1983)111<0430:AUBCPI>2.0.CO;2.
- [33] D. A. Kopriva. “Metric Identities and the Discontinuous Spectral Element Method on Curvilinear Meshes”. In: *Journal of Scientific Computing* 26.3 (2006), pp. 301–327. DOI: 10.1007/s10915-005-9070-8.
- [34] D. A. Kopriva. “Spectral Element Methods”. In: *Implementing Spectral Methods for Partial Differential Equations: Algorithms for Scientists and Engineers*. Dordrecht: Springer Netherlands, 2009, pp. 293–354. DOI: 10.1007/978-90-481-2261-5_8.
- [35] J. F. B. M. Kraaijevanger. “Contractivity of Runge-Kutta methods”. In: *BIT Numerical Mathematics* 31.3 (1991), pp. 482–528. DOI: 10.1007/BF01933264.

- [36] Y. Kuya, K. Totani, and S. Kawai. “Kinetic energy and entropy preserving schemes for compressible flows by split convective forms”. In: *Journal of Computational Physics* 375 (2018), pp. 823–853. DOI: 10.1016/j.jcp.2018.08.058.
- [37] Y. Liu, W. Guo, Y. Jiang, and M. Zhang. “Structure-preserving nodal DG method for the Euler equations with gravity: well-balanced, entropy stable, and positivity preserving”. In: *Journal of Computational Physics* 537 (2025), p. 114095. DOI: 10.1016/j.jcp.2025.114095.
- [38] G. Mengaldo, D. De Grazia, D. Moxey, P. Vincent, and S. Sherwin. “Dealiasing techniques for high-order spectral element methods on regular and irregular grids”. In: *Journal of Computational Physics* 299 (2015), pp. 56–81. DOI: 10.1016/j.jcp.2015.06.032.
- [39] A. Müller, M. A. Kopera, S. Marras, L. C. Wilcox, T. Isaac, and F. X. Giraldo. “Strong scaling for numerical weather prediction at petascale with the atmospheric model NUMA”. In: *The International Journal of High Performance Computing Applications* 33.2 (2019), pp. 411–426. DOI: 10.1177/1094342018763966.
- [40] G. Orlando, T. Benacchio, and L. Bonaventura. “An IMEX-DG solver for atmospheric dynamics simulations with adaptive mesh refinement”. In: *Journal of Computational and Applied Mathematics* 427 (2023), p. 115124. DOI: 10.1016/j.cam.2023.115124.
- [41] J.-P. Pinty, R. Benoit, E. Richard, and R. Laprise. “Simple Tests of a Semi-Implicit Semi-Lagrangian Model on 2D Mountain Wave Problems”. In: *Monthly Weather Review* 123.10 (1995), pp. 3042–3058. DOI: 10.1175/1520-0493(1995)123<3042:STOASI>2.0.CO;2.
- [42] C. Rackauckas and Q. Nie. “DifferentialEquations.jl – A Performant and Feature-Rich Ecosystem for Solving Differential Equations in Julia”. In: *Journal of Open Research Software* 5.1 (2017), p. 15. DOI: 10.5334/jors.151.
- [43] H. Ranocha. “Comparison of Some Entropy Conservative Numerical Fluxes for the Euler Equations”. In: *Journal of Scientific Computing* 76.1 (2018), pp. 216–242. DOI: 10.1007/s10915-017-0618-1.
- [44] H. Ranocha. “Entropy Conserving and Kinetic Energy Preserving Numerical Methods for the Euler Equations Using Summation-by-Parts Operators”. In: *Spectral and High Order Methods for Partial Differential Equations ICOSAHOM 2018*. Ed. by S. J. Sherwin, D. Moxey, J. Peiró, P. E. Vincent, and C. Schwab. Vol. 134. Lecture Notes in Computational Science and Engineering. Cham: Springer, 2020, pp. 525–535. DOI: 10.1007/978-3-030-39647-3_42.
- [45] H. Ranocha and G. J. Gassner. “Preventing Pressure Oscillations Does Not Fix Local Linear Stability Issues of Entropy-Based Split-Form High-Order Schemes”. In: *Communications on Applied Mathematics and Computation* 4.3 (2022), pp. 880–903. DOI: 10.1007/s42967-021-00148-z.
- [46] H. Ranocha. “Generalised Summation-by-Parts Operators and Entropy Stability of Numerical Methods for Hyperbolic Balance Laws”. PhD thesis. TU Braunschweig, Feb. 2018.
- [47] H. Ranocha. “Shallow water equations: split-form, entropy stable, well-balanced, and positivity preserving numerical methods”. In: *GEM - International Journal on Geomathematics* 8.1 (2017), pp. 85–133. DOI: 10.1007/s13137-016-0089-9.
- [48] H. Ranocha, M. Schlottke-Lakemper, J. Chan, A. M. Rueda-Ramírez, A. R. Winters, F. Hindenlang, and G. J. Gassner. “Efficient implementation of modern entropy stable and kinetic energy preserving discontinuous Galerkin methods for conservation laws”. In: *ACM Transactions on Mathematical Software* 49 (4 Sept. 2023). DOI: 10.1145/3625559.
- [49] H. Ranocha, M. Schlottke-Lakemper, A. R. Winters, E. Faulhaber, J. Chan, and G. J. Gassner. “Adaptive numerical simulations with Trixi.jl: A case study of Julia for scientific computing”. In: *Proceedings of the JuliaCon Conferences* 1.1 (Jan. 2022), p. 77. DOI: 10.21105/jcon.00077.
- [50] A. M. Rueda-Ramírez and G. J. Gassner. “A flux-differencing formula for split-form summation by parts discretizations of non-conservative systems: Applications to subcell limiting for magneto-hydrodynamics”. In: *Journal of Computational Physics* 496 (2024), p. 112607. DOI: 10.1016/j.jcp.2023.112607.
- [51] A. M. Rueda-Ramírez, S. Hennemann, F. J. Hindenlang, A. R. Winters, and G. J. Gassner. “An entropy stable nodal discontinuous Galerkin method for the resistive MHD equations. Part II: Subcell finite volume shock capturing”. In: *Journal of Computational Physics* 444 (2021), p. 110580. DOI: 10.1016/j.jcp.2021.110580.
- [52] M. Schlottke-Lakemper, A. R. Winters, H. Ranocha, and G. J. Gassner. “A purely hyperbolic discontinuous Galerkin approach for self-gravitating gas dynamics”. In: *Journal of Computational Physics* 442 (June 2021), p. 110467. DOI: 10.1016/j.jcp.2021.110467.

- [53] C. Schär, D. Leuenberger, O. Fuhrer, D. Lüthi, and C. Girard. “A New Terrain-Following Vertical Coordinate Formulation for Atmospheric Prediction Models”. In: *Monthly Weather Review* 130.10 (2002), pp. 2459–2480. DOI: 10.1175/1520-0493(2002)130<2459:ANTFVC>2.0.CO;2.
- [54] N. Shima, Y. Kuya, Y. Tamaki, and S. Kawai. “Preventing spurious pressure oscillations in split convective form discretization for compressible flows”. In: *Journal of Computational Physics* 427, 110060 (Feb. 2021), p. 110060. DOI: 10.1016/j.jcp.2020.110060.
- [55] B. Sjögren and H. Yee. “High order entropy conservative central schemes for wide ranges of compressible gas dynamics and MHD flows”. In: *Journal of Computational Physics* 364 (2018), pp. 153–185. DOI: 10.1016/j.jcp.2018.02.003.
- [56] R. B. Smith. “The Influence of Mountains on the Atmosphere”. In: *Advances in Geophysics* 21 (1979), pp. 87–230.
- [57] A. N. Souza, J. He, T. Bischoff, M. Waruszewski, L. Novak, V. Barra, T. Gibson, A. Sridhar, S. Kandala, S. Byrne, L. C. Wilcox, J. Kozdon, F. X. Giraldo, O. Knuth, J. Marshall, R. Ferrari, and T. Schneider. “The Flux-Differencing Discontinuous Galerkin Method Applied to an Idealized Fully Compressible Nonhydrostatic Dry Atmosphere”. In: *Journal of Advances in Modeling Earth Systems* 15.4 (2023). e2022MS003527 2022MS003527, e2022MS003527. DOI: 10.1029/2022MS003527.
- [58] E. Tadmor. “Entropy stability theory for difference approximations of nonlinear conservation laws and related time-dependent problems”. In: *Acta Numerica* 12 (2003), pp. 451–512. DOI: 10.1017/S0962492902000156.
- [59] E. Tadmor. “The numerical viscosity of entropy stable schemes for systems of conservation laws. I”. In: *Mathematics of Computation* 49.179 (1987), pp. 91–103. DOI: 10.1090/S0025-5718-1987-0890255-3.
- [60] P. Ullrich, C. Jablonowski, K. Reed, C. Zarzycki, P. Lauritzen, R. Nair, J. Kent, and A. Verlet-Banide. *Dynamical core model intercomparison project (DCMIP2016) test case document*. <https://github.com/ClimateGlobalChange/DCMIP2016>. 2016.
- [61] P. A. Ullrich, T. Melvin, C. Jablonowski, and A. Staniforth. “A proposed baroclinic wave test case for deep- and shallow-atmosphere dynamical cores”. In: *Quarterly Journal of the Royal Meteorological Society* 140.682 (2014), pp. 1590–1602. DOI: 10.1002/qj.2241.
- [62] P. A. Ullrich, D. R. Reynolds, J. E. Guerra, and M. A. Taylor. “Impact and importance of hyperdiffusion on the spectral element method: A linear dispersion analysis”. In: *Journal of Computational Physics* 375 (2018), pp. 427–446. DOI: 10.1016/j.jcp.2018.06.035.
- [63] M. Waruszewski, J. E. Kozdon, L. C. Wilcox, T. H. Gibson, and F. X. Giraldo. “Entropy stable discontinuous Galerkin methods for balance laws in non-conservative form: Applications to the Euler equations with gravity”. In: *Journal of Computational Physics* 468 (2022), p. 111507. DOI: 10.1016/j.jcp.2022.111507.
- [64] A. R. Winters, C. Czernik, M. B. Schily, and G. J. Gassner. “Entropy stable numerical approximations for the isothermal and polytropic Euler equations”. In: *BIT Numerical Mathematics* 60.3 (2020), pp. 791–824. DOI: 10.1007/s10543-019-00789-w.
- [65] A. R. Winters, D. Derigs, G. J. Gassner, and S. Walch. “A uniquely defined entropy stable matrix dissipation operator for high Mach number ideal MHD and compressible Euler simulations”. In: *Journal of Computational Physics* 332 (2017), pp. 274–289. DOI: 10.1016/j.jcp.2016.12.006.
- [66] A. R. Winters, D. A. Kopriva, G. J. Gassner, and F. Hindenlang. “Construction of Modern Robust Nodal Discontinuous Galerkin Spectral Element Methods for the Compressible Navier–Stokes Equations”. In: *Efficient High-Order Discretizations for Computational Fluid Dynamics*. Springer, 2021, pp. 117–196.
- [67] A. R. Winters, R. C. Moura, G. Mengaldo, G. J. Gassner, S. Walch, J. Peiro, and S. J. Sherwin. “A comparative study on polynomial dealiasing and split form discontinuous Galerkin schemes for under-resolved turbulence computations”. In: *Journal of Computational Physics* 372 (2018), pp. 1–21. DOI: 10.1016/j.jcp.2018.06.016.
- [68] J. Yu and H. S. Jan. “A Study of Several Artificial Viscosity Models within the Discontinuous Galerkin Framework”. In: *Communications in Computational Physics* 27.5 (2020), pp. 1309–1343. DOI: 10.4208/cicp.OA-2019-0118.